Maria Marta Oliveira Antunes dos Santos

Licenciatura em Engenharia Biomédica

Study of the electromyographic signal dynamic behavior in Amyotrophic Lateral Sclerosis (ALS)

Dissertação para obtenção do Grau de Mestre em
Engenharia Biomédica

Orientadora : Carla Quintão, Professora Auxiliar, Faculdade de Ciências e Tecnologia da Universidade Nova de Lisboa

Co-orientador : Hugo Gamboa, Professor Auxiliar, Faculdade de Ciências e Tecnologia da Universidade Nova de Lisboa

Júri:

Presidente: Doutor Mário Forjaz Secca

Arguente: Doutor Alexandre Freire de Andrade

Vogal: Doutora Carla Quintão

FACULDADE DE CIÊNCIAS E TECNOLOGIA
UNIVERSIDADE NOVA DE LISBOA

October, 2014

Study of the electromyographic signal dynamic behavior in Amyotrophic Lateral Sclerosis (ALS)

À minha família.

Acknowledgements

First I thank my supervisor, Professor Carla Quintão, for her guidance and patience, her vigorous spirit and knowledge. I am very grateful for her availability, ideas, motivation and encouragement. I thank my co-supervisor, Professor Hugo Gamboa, who offered me new ideas and solutions. I thank Doctor Professor Mamede de Carvalho and Doctor Susana Pinto for their collaboration, making possible to perform acquisitions from patients at Hospital Sta. Maria. I thank Ricardo Gomes for his patience and ideas, and all the staff of *PLUX – Wireless Biosignals*, S. A., for receiving me every day.

A very big thank you to Luísa Gomes, for her help, patience and opinions; for the everyday conversations we shared; these years would not have been the same without her. To Inês Vale, Inês Silva, David Branha and Catarina Cavaco I thank for these wonderful years; their friendship, support and motivation are essential. I also thank my oldest friends, who in spite of sometimes are away, are always in my heart.

Lastly, I thank my family. I thank my parents for their unconditional love, motivation and support, and for making me feel I can do everything if I work for it. I thank my sister for her love and admiration. To my uncle and aunt, an enormous thank you for offering me their home, love and protection; these years would not have been the same without their support. I thank my grandparents for their concern and belief in me.

Abstract

Amyotrophic Lateral Sclerosis (ALS) is a neurodegenerative disease characterized by motor neurons degeneration, which reduces muscular force, being very difficult to diagnose. Mathematical methods are used in order to analyze the surface electromiographic signal's dynamic behavior (Fractal Dimension (FD) and Multiscale Entropy (MSE)), evaluate different muscle group's synchronization (Coherence and Phase Locking Factor (PLF)) and to evaluate the signal's complexity (Lempel-Ziv (LZ) techniques and Detrended Fluctuation Analysis (DFA)). Surface electromiographic signal acquisitions were performed in upper limb muscles, being the analysis executed for instants of contraction for ipsilateral acquisitions for patients and control groups. Results from LZ, DFA and MSE analysis present capability to distinguish between the patient group and the control group, whereas coherence, PLF and FD algorithms present results very similar for both groups. LZ, DFA and MSE algorithms appear then to be a good measure of corticospinal pathways integrity. A classification algorithm was applied to the results in combination with extracted features from the surface electromiographic signal, with an accuracy percentage higher than 70% for 118 combinations for at least one classifier. The classification results demonstrate capability to distinguish members between patients and control groups. These results can demonstrate a major importance in the disease diagnose, once surface electromyography (sEMG) may be used as an auxiliary diagnose method.

Keywords: Amyotrophic Lateral Sclerosis (ALS), Coherence, Phase Locking Factor (PLF), Fractal Dimension (FD), Lempel-Ziv (LZ), Detrended Fluctuation Analysis (DFA), Multiscale Entropy (MSE) , Surface Electromyography (sEMG), Ipsilateral, Classification.

Resumo

A Esclerose Lateral Amiotrófica (ELA) é uma doença neurodegenerativa caracterizada pela degeneração progressiva de neurónios motores, o que reduz a força muscular, sendo muito difícil de ser diagnosticada. São usados métodos matemáticos de forma a caracterizar o sinal eletromiográfico de superfície (sEMG) de pacientes com ELA, com o objetivo de analisar o comportamento dinâmico do sinal (Dimensão Fractal (DF) e Multiscale Entropy (MSE)), avaliar a sincronização de diferentes grupos musculares (Coerência e Phase Locking Factor (PLF)) e avaliar a complexidade do sinal (técnicas de Lempel-Ziv (LZ) e Detrended Fluctuation Analysis (DFA)). A aquisição de sEMG foi feita em músculos dos membros superiores, sendo a análise feita para momentos de contração para aquisições ipsilaterais tanto para o grupo de pacientes como para o grupo de controlo. Os resultados das análises de LZ, DFA e MSE apresentam capacidade de distinção entre o grupo de pacientes e o grupo de controlo, enquanto que os algoritmos de coerência, PLF e DF apresentam resultados muito similares para ambos os grupos. Os algoritmos de LZ, DFA e MSE aparentam, então, ser bons indicadores da integridade de percursos corticoespinhais. Um algoritmo de classificação foi também aplicado aos resultados destes algoritmos em conjunto com *features* extraídas do sinal de sEMG, com uma percentagem de acerto de 70% para 118 combinações para pelo menos um classificador. Os resultados da classificação demonstram capacidade de distinção entre os grupos de pacientes e controlo. Estes resultados podem demonstrar-se importantes no diagnóstico da doença, sendo que se poderá passar a usar electromiografia de superfície como método auxiliar de diagnóstico.

Palavras-chave: Esclerose Lateral Amiotrófica (ELA), Coerência, Phase Locking Factor (PLF), Dimensão Fractal (DF), técnicas de Lempel-Ziv (LZ), Detrended Fluctuation Analysis (DFA), Multiscale Entropy (MSE), Electromiografia de superfície (sEMG), Ipsilateral, Classificação.

Contents

List of Figures

List of Tables

Acronyms

ALS Amyotrophic Lateral Sclerosis

AP Action Potential

B Bulbar

CNS Central Nervous System

DC Direct Current Component

DFA Detrended Fluctuation Analysis

ECG Electrocardiogram

EEG Electroencephalogram

EMG Electromyography

FD Fractal Dimension

FFT Fast Fourier Transform

FPs Fasciculation Potentials

IDFT Discrete Inverse Fourier Transform

LLL Left Lower Limb

LMN Lower Motor Neuron

LUL Left Upper Limb

LZ Lempel-Ziv

MFL Maximum Fractal Length

MND Motor Neuron Disease

MR Magnetic Resonance

MSE Multiscale Entropy

MU Motor Unit

MUAP Motor Unit Action Potential

MUNE Motor Unit Number Estimation

MUPs Motor Unit Potentials

NCS Nerve Conduction Studies

NFFT Nonequispaced Fast Fourier Transform

PLF Phase Locking Factor

PLS Primary Lateral Sclerosis

RLL Right Lower Limb

RMS Root Mean Square

RUL Right Upper Limb

sEMG Surface Electromyography

UL Upper Limbs

UMN Upper Motor Neuron

1

Introduction

1.1 Motivation

Amyotrophic Lateral Sclerosis (ALS) is a neurodegenerative disease which is characterized by motor neurons progressive degeneration [5, 6, 7]. This is a fatal and very progressive disease, which is responsible for abnormal motor activity [5, 6, 7, 8, 9]. However, neurodegeneration is believed to begin long before the development of any symptoms [10]. Therefore, ALS is very difficult to diagnose and to control. On top of that, there aren't any available curative treatments for this disease, as well as a reliable biomarker of disease activity and progression [6, 9].

This disease incidence, which affects people throughout the world, is not exactly known [9]. Population studies including European citizens have demonstrated an uniform incidence of 2.16 per 100000 person-years, with slightly higher incidence among men than women [6, 9]. More recent studies established an approximately 1.5 per 100000 worldwide incidence [7].

At the present time ALS management is focused on palliative care and symptomatic treatments, such as the development and application of supportive therapies in order to improve patients' quality of life (as well as their families') and survival. Despite the existence of many clinical trials, within an effort to understand the complexity of this disease and to delay its progression (e.g. through drug development) ALS is still very difficult to diagnose [5, 6, 9]. Therefore, this project intends to use mathematical methods, such as Coherence, Phase Locking Factor (PLF), FD, LZ techniques, Correlations, Fourier analysis, DFA and MSE to characterize ALS patients' Surface Electromyography (sEMG) signal, to analyze the signal's chaotic behavior and its complexity and to evaluate different muscle groups synchronization.

1.2 Objectives

The purpose of this thesis is to study the electrical activity of different muscle groups both in ALS patients and in a control group.

Surface electrodes will be used to acquire a surface electromyographic (sEMG) signal from both groups, which will be processed and analyzed. Physiological features will be extracted and variations in the electric signal between both groups will be studied.

The algorithms used to process the signal include:

- Coherence analysis to analyze frequency correlations between different muscle groups;
- Phase Locking Factor calculations to detect synchronization between different muscle groups;
- Fractal Dimension and Multiscale Entropy to evaluate the signal's chaotic behavior;
- Lempel-Ziv and Detrended Fluctuation Analysis methods to estimate the signal's complexity.

There will also be applied classification algorithms in order to distinguish both groups. These algorithms are: k-Nearest Neighbor, Decision Tree, Random Forest, AdaBoost and Naïve Bayes.

Ultimately, the aim is to determine if an individual is affected by a neurodegenerative disorder, particularly ALS, evaluate the disorder stages of progression, as well as distinguish between healthy individuals and individuals affected by this disease. Therefore, this project requires an acquisition protocol, signal recordings and signal processing.

1.3 State-of-the-art

Considering the lack of existence of a biologic marker for ALS, this disease is diagnosed mostly by clinical criteria. Although some patients may present symptoms consistent with ALS, it is necessary to exclude other possible diagnosis, such as demyelinating motor neuropathies, among others [7, 9, 11]. To diagnose ALS, several rating scales have been developed in an effort to classify patients according to diagnose certainty, using a combination of upper and lower motor neuron signs. These include the Appel amyotrophic lateral sclerosis rating scale, the amyotrophic lateral sclerosis functional rating scale and El Escorial diagnostic criteria for amyotrophic lateral sclerosis [5, 9, 12]. This latter ratting scale, in combination with the Awaji modifications to the diagnostic categories of the revised El Escorial criteria, is the most sensitive and specific criteria regarding ALS's diagnostic [7, 11]. However, despite very helpful, these criteria have revealed some difficulties regarding lower motor neuron lesions detection, since this criteria takes more into account clinical signs than electrodiagnostic findings [7, 13]. The incapability to assess the corticospinal tract is also a restraint regarding ALS diagnostic. In spite of the

Babinski sign and hyperreflexia may be indicators of impairment in corticospinal track, they can't alone reflect such damage [14].

Several techniques have been used in an effort to detect, evaluate and quantify motor degeneration in ALS, as well as exclude other disorders with identical symptoms. These include Needle Electromyography (EMG), Nerve Conduction Studies (NCS), Motor Unit Number Estimation (MUNE), used mainly in the research setting, Neurophysiological Index, Transcranial Magnetic Stimulation and Neuroimaging techniques, such as Magnetic Resonance Spectroscopy and Diffusion Tensor Magnetic Resonance (MR) Tractography, among others. In addition to these techniques, Sniff Nasal Pressure and Maximum Voluntary Isometric Contraction have also been investigated though they can't be used as a test for all patients. Aside from these techniques, which can be used as disease progression markers, disease modifying pharmacological therapies have been investigated as well, although the results remain elusive. However, at present time, Riluzole is the only pharmacological agent with modest effect, and its effects could be considerately better if administrated early in the disease course [5, 7, 9, 11, 14, 15] .

Upper Motor Neuron integrity can be evaluated through the investigation of oscillatory activity propagation. Rhythmic activity in the alpha (8 - 12 Hz) and beta (15–30 Hz) frequency bands can be recorded from the motor cortex and coherence may be computed. The results of this coherence analysis evidence synchronization between cortex and contralateral EMG in the beta band, which suggests that these oscillations are conveyed from cortex to muscle. Therefore, it is believed that pyramidal tract neurons are related to generation and propagation of beta band oscillations [14]. Beta band coupling (in normal subjects) can be observed between different muscles as well – intermuscular coherence – [14, 16], which reveals the existence of a shared cortical drive. Moreover, coherence between muscles and the motor cortex is a measure of oscillatory coupling between electromyographic discharge and the central nervous system motor elements, whereas the phase difference provides an estimate of the temporal delay between cortex and EMG [17]. Also, during steady muscle contraction, it is observed maximum intermuscular coherence. Intermuscular coherence appears to be dependent on supraspinal structures, since it disappears after impairment of these structures. However, it doesn't appear to depend on anterior horn cells. Beta band and intermuscular coherence have also been proved to be greatly influenced by sensory afferents [14]. In fact, cortical coherence has been proved to involve transmission in both descending (motor) and ascending (sensory) direction [18]. Concerning the alpha band, it was stated by *Farmer et al.* that physiological tremor of approximately 10 Hz has been associated to Motor Unit (MU) synchrony at 8-12 Hz [19, 16].

While performing a task, the involved control process depends on the task's frequency. Hence, corticospinal coherence may involve not only the corticospinal tract, but also different pathways. Motor Unit recruitment control processes are also influenced by the force's output magnitude [16, 18].

Coherence at frequencies from 1 Hz to 45 Hz (in adults) have been associated to Motor Unit firing recorded from pairs of cocontracting muscles, being maximal in a low frequency range (1-12 Hz) and in a high frequency range (16-32 Hz, with maxima at approximately 20 Hz). Moreover, cortical coherence at approximately 20 Hz, as well as Motor Unit synchrony are concomitant with important common drive, which conducts to coactivation of closely related muscles [19]. *Farmer et al.* [19] have also suggested that increased speed and accuracy when performing a motor task and more efficient Motor Unit recruitment are associated with a 20 Hz coherence as well.

Either normal or pathological signals can be characterized by means of the FD study of an EMG signal. Small changes in the FD of these signals are indicators of muscle activation in a linear way. This muscle activation is related with voluntary contraction since it can be measured as a fraction of its maximum value. Flexion-extension speeds and load are linearly related with FD as well. MU recruitment patterns complexity can also be quantified using FD [20]. *Arjunan et al.* [21] confirmed these findings observing a relationship between muscle contraction complexity and FD. Therefore, changes in a muscle shape and contraction may influence this complexity, and consequently the FD as well. As a matter of fact, small changes of muscle contraction are concomitant with small variations of FD while high level of muscle contraction or stretch presents a higher impact on this measure [20]. *Arjunan et al.* [22] reached the conclusion that the strength of a muscle's contraction is better estimated based on Maximum Fractal Length (MFL), even for very small muscle contraction strength, rather than FD (which is confirmed in [20] where it is proposed the use of the signal's overall length as a measure of muscle activity) or other features such as Variance (VAR), Waveform Length (WL) and Root Mean Square (RMS). Accordingly, *Arjunan et al.* [21] also evidenced that the contraction's strength of the associated muscles is related to MFL. These authors have applied fractal density and MFL to the identification of a set of finger-and-wrist flexion-based actions in conditions of very weak muscle activity. They validated this system and suggested it would be useful for a human computer interface or the control of a prosthetic hand [21].

The LZ complexity is a measure used to identify and quantify deterministic complexity in signals, such as sEMG, evaluating the generation rate of distinct deterministic patterns within a signal. This measure only considers the number of distinct patterns, being insensitive to the total number of patterns within a signal. [23]. It is described in literature [23, 24] that a multi-level symbolizing approach of this algorithm can outperform a binary approach, namely in terms of correlation, since the latter approach appears to cause a false sense of complexity in low amplitude signals. *Talebinejad et al.* [23] confirmed that the LZ complexity measure, which decreases in a situation of fatigue, is reliable regarding fatigue estimation, and stressed its interest concerning the analysis of dynamic contractions, since it demonstrates larger sensitivity to fatigue rather than muscle length or force. These authors also found evidences that single or superimposed deterministic Motor Unit Action Potential (MUAP) patterns can be tracked with the application of this feature, which reflects MUAPs duration and creation rate in a sEMG signal. Since the

LZ complexity measure reflects variations in synchronization of firing MUs and in muscle fiber conduction velocity consistent with situations of fatigue, this feature is considered to have higher performance when compared with median frequency, since median frequency is not reliable to what concerns to synchrony. These authors have also confirmed these results with their previous work with multi-fractal Detrended Fluctuation Analysis (DFA). The LZ measure is a well suited feature regarding sEMG analysis, particularly during dynamic contractions (highly non-stationary signal), since this feature doesn't make any assumption of stationarity (rather than other analysis techniques such as power spectrum estimations, among others) [23].

Phinyomark et al. [25] proposed the use of DFA in order to study EMG signals, since they exhibit complex and nonlinear properties. They evidenced the efficacy of this method to discriminate upper-limb movements. These authors also showed that the DFA method outperforms other methods (e. g. the correlation dimension method and the Higuchi method), since it is a stable technique to quantify fractality and to establish self-similarity, being a robust method in the presence of nonstationarity time series and trends. The DFA method is also a suitable tool regarding the characterization of short-time nonstationary EMG time series. This method has also been used as a fatigue index in previous studies [25].

Entropy is a feature which can detect and quantify differences in the EMG signal amplitude distributions due to neuromuscular conditions (pathology) [26]. This feature has been successfully applied to physiological signals, in order to quantify their degree of complexity. Multiscale Entropy (MSE) has been proved to be more effective than Single-scale Entropy in this quantification, since it considers multiple spatiotemporal scales [27, 28]. *Thuraisingham et al.* [28] analyzed a deterministic chaotic system (the Lorentz equation) and evinced that the MSE signature obtained from a time series is dependent of the sampling time interval, the oscillation's period and the correlation time. For instance, sampling rate can affect MSE signature by causing decorrelation and suppress periodicities. Moreover, the time scales under consideration influence greatly the degree of complexity. So, if the sampling time is greater than the correlation time and the period of probable nonlinear frequencies, chaotic time series (with or without nonlinear frequencies) exhibit the same MSE signature as white noise (uncorrelated fluctuation) [28]. If the sampling time is smaller than the correlation time in the sampled data (or the correlation time is greater than periods of possible nonlinear frequencies), the Sample Entropy will firstly increase (because of decorrelation) and subsequently decrease according to the law of the averages.

Several studies have been conducted in order to distinguish individuals in groups, such as age, gender and to identify injury mechanism characteristics [29]. Musculoskeletal system disorders may be evaluated using EMG devices. This technique may be applied to several fields, such as in providing assistance for the disabled, rehabilitation training and also in device control (e. g. control of game devices) [30]. Therefore, algorithms based on pattern recognition methods are essential, and in order to find the most

reliable algorithm it is necessary to apply a classification process and to compare different classifiers [29, 30]. However, the analyzed features have great influence on the results [29]. Considering feature extraction, the size of the time window may also influence the results, being an important factor in the sampling parameters for EMG signal processing [30].

k-Nearest Neighbor is a relatively simple and fast algorithm, important characteristics in the classification process [30]. Decision Tree methods have also been used for dealing with classification problems in various domains, such as pattern recognition, data mining, web mining and signal processing, among others. However, standard Decision Tree algorithms can only handle discrete attributes [31]. The Decision Tree algorithm has usually good performance for large data sets in a short time [32]. Random Forest algorithm has been tested with real and simulated data sets. The results have been proven to be very accurate. This algorithm is fast, versatile and can be applied to very large data sets. It has also been shown its robustness against noise in the outcome compared with several other methods [33]. Discrimination between subject or patient group concerning age, gender and injuries in athletes has been proven to be effective using a classification approach with generic features and AdaBoost [29]. Naïve Bayes method has shown to be competitive among much sophisticated induction algorithms concerning experiments on real world data, despite the assumption of conditional independence [31].

1.4 Thesis Overview

This work is structured in different chapters. The first two chapters contain literature review concerning ALS disease, EMG signals, signal analysis, coherence, PLF, FD, LZ, DFA and MSE algorithms and classification. Therefore, the first chapter includes the state-of-the-art, as well as the main objectives of this thesis, and the second chapter contains the theoretical background that supports it. The third chapter explains the acquisition protocol and the recording device, discussing both groups description as well. Chapter 4 refers to high level and low level signal processing, including the explanation of all the algorithms referred above, as well as algorithm validation (noise generation and synthetic signals). Chapter 5 presents and discusses the obtained results regarding all algorithms, including also the algorithm validation results. Chapter 6 presents the conclusions obtained from the results analysis. There are three appendixes in this work: Appendix A contains more explanatory coherence and PLF graphics which complement the graphics presented in Chapter 5; Appendix B contains the results obtained with the classification algorithm; Appendix C, which contains an abstract and a poster presented in a conference in the context of this research work, and another abstract of the paper submitted in another conference. This thesis was written using LATEX and all the acquisitions were analyzed using Python software.

2

Theoretical background

2.1 Scientific support

2.1.1 Amyotrophic Lateral Sclerosis (ALS)

ALS is a neurological and rapid progressive degenerative disease, also known as Lou Gehrig disease or Motor Neuron Disease (MND). This disorder is characterized by both Upper and Lower Motor Neurons degeneration, involving brainstem and also multiple spinal cord innervation regions. In fact, corticospinal tract integrity may be damaged in any region from layer V pyramidal neurons from the motor cortex, where UMN (also known as Betz cells) are located, to the anterior horn of the spinal cord, where LMN are located [6, 9, 14]. Thus, this disorder is characterized according to the affected neurological regions: bulbar, cervical, thoracic and lumbrosacral [5, 12, 14]. Clinical manifestations of ALS are associated to each one of these regions, and the identification of different phenotypes has significant importance regarding patients' prognosis and survival. Some adverse prognostic indicators include reduced time among first symptoms and disease presentation, low forced vital capacity and increased age of onset [5].

ALS patients may experience symptoms such as muscle atrophy, cramps, spasticity and fasciculations, as previously referred [5, 7, 8, 9]. Moreover, they typically present fatigue, quickly progressive weakness and reduced exercise capacity with loss of voluntary movement, since all voluntary muscles innervated by MUs are affected in this disorder. Other common features usually exhibited in ALS are dysphagia (difficulty in swallowing), dyspnea (difficulties in breathing) and dysarthria (difficulties in speaking). Besides these direct symptoms, ALS patients may experience pain and psychological and

sleep disturbances, among other indirect symptoms which are a repercussion of the direct ones. After the first symptoms, death may occur within 3 – 5 years for most of the patients [5, 6, 7, 9] .

While 90% of cases of ALS are sporadic or idiopathic, approximately 10% of ALS cases are familial [5, 6, 7, 9]. However, although several theories concerning ALS causes and pathogenesis have been studied, this disease etiology still remains poorly understood [5, 6, 7]. Familial ALS is related most commonly with autosomal-dominant patterns, but also with X-linked and autosomal recessive patterns. More than 75 causative mutations of ALS have been described over the years, being a point mutation in the copper/zinc ion-binding superoxide dismutase (SOD1) the first one to be reported [5, 7, 9]. These mutations in SOD1 gene provoke a toxic gain of function of the SOD1 protein, instead of a reduction of activity of the same protein, as previously supposed. However, the most likely common mutation recently described is a hexanucleotide repeat expansion of the chromosome 9 open reading frame 72 (C9orf72) gene. These genes are not only associated with ALS familial cases, but also with a reduce number of apparently sporadic cases [7, 9]. ALS has also been linked with environmental and occupational risk factors, including heavy-metal toxic effects, neurotoxins military service, cigarette smoking, agricultural or factory work and physical exertion. Nevertheless, it wasn't determined a definite causal relationship with any of these factors [5, 6, 7, 9]. Other pathogenic hypothesis regarding this disorder are mitochondrial dysfunction, increased intracellular calcium, autophagy, sodium/potassium ion pump dysfunction, disrupted axon transport systems and protein disaggregation. The latter is associated with mutations in the genes for fused in sarcoma (FUS) and TAR DNA binding protein-43 (TDP-43). Angiogenin (ANG, ribonuclease, RNase A family, 5) and optineurin (OPTN) are also associated to clinical phenotype. TDP-43, FUS and ANG are involved in RNA trafficking [7, 9]. In addition to the previous hypothesis, glutamate-induced excitotoxicity can incite neurodegeneration. In literature [9] two theories are described for the beginning of this disorder, considering the mechanism of MU degeneration mediated by glutamate-induced excitotoxicity. They are the "dying - forward" and the "dying - back" hypothesis. The former suggests ALS to be a corticomotorneurons disorder which connect monosynaptically with anterior horn cells, mediating anterograde degeneration of anterior horn cells via glutamate excitotoxicity. The latter postulates the beginning of ALS to be at the neuromuscular junction or within the muscle cells. In particular, there is a motor neurotrophic hormone deficiency, which is usually released by postsynaptic cells and retrogradely transported up the presynaptic axon to the cell body where it exercises its effects.

Riluzole (Rilurek), which is a glutamate release inhibitor, is at this point the only licensed diseased-modifying management for ALS, and it is capable of extend patients survival by 3-6 months. Conversely, attempts made in order to develop antioxidants strategies regarding ALS have proved to be unsatisfactory [5, 6, 7, 9].

2.1.2 Propagation of nervous impulses, motor units and action potentials

Motor Neurons are the motor component of the Central Nervous System (CNS) and can be separated in Upper Motor Neurons (UMNs) and Lower Motor Neurons (LMNs).

UMNs convey impulses for voluntary motor activity from the motor cortex or the brainstem through descending pathways until a specific nerve root from the ventral horn of the spinal cord. At this point, LMNs carry the information from UMNs to muscle fibers. This information is transmitted by means of synapses: the neurotransmitter glutamate transmits the impulse from UMNs to LMNs and acetylcholine transmits the impulse from LMNs to muscle fibers. Figure 2.1 shows a schematic representation of the lateral cortical spinal tract.

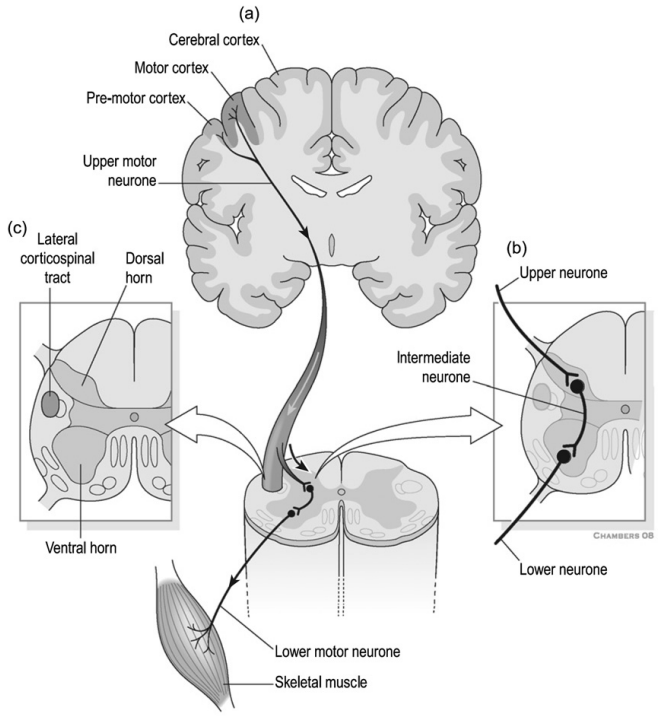

Figure 2.1: Lateral cortical spinal tract. (a) Descending motor pathways carry information from the brain to the spinal cord. (b) Region where UMNs interdigitate with LMNs. LMNs carry the information from UMNs to the muscles. (c) Location of the lateral cortical spinal tract in the spinal cord [1].

LMNs can be classified in Alpha Motor Neurons (α-MNs) and Gamma Motor Neurons (γ-MNs), based on the muscle fiber type they innervate. α-MNs innervate extrafusal muscle fibers, which are involved in muscle contraction. γ-MNs innervate intrafusal muscle fibers, which are responsible for sensing body position (proprioception).

An Alpha Motor Neuron cell body, the axon and all branches plus the skeletal muscle fibers innervated by that motor axon constitute a Motor Unit (MU). MUs are the elementary component of muscular strength, and must fire repeatedly to maintain or increase the forced produced by a muscle [2, 34]. Figure 2.2 shows a schematic representation of a MU.

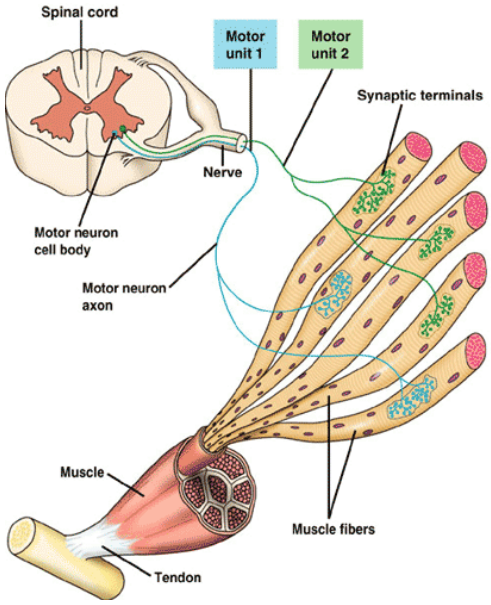

Figure 2.2: Motor Unit: a Motor Neuron with several branches, each one of them terminating at different muscle fibers of the same type. This terminal branches are typically in a 'One-To-One' relationship with the muscle fibers (a muscle fiber receives only a terminal branch, and a terminal branch innervates only a muscle fiber) [2, 3, 4].

An Action Potential (AP) is an electrical signal conducted along muscle fibers by which information is conveyed in the nervous system by means of ionic transport along the membrane. The combination of these APs along all the muscle fibers of a single MU is called the MUAP [35]. CNS sends this electrical signal which reach the α-MN responsible for initiating muscle contraction and spreads across muscle fibers, as a result of a series of electrically measurable de-polarization and re-polarization events (AP). If the nerve impulse arrives more often, the intensity of muscle contraction is greater [2]. Figure 2.3 shows a schematic representation of a single action potential.

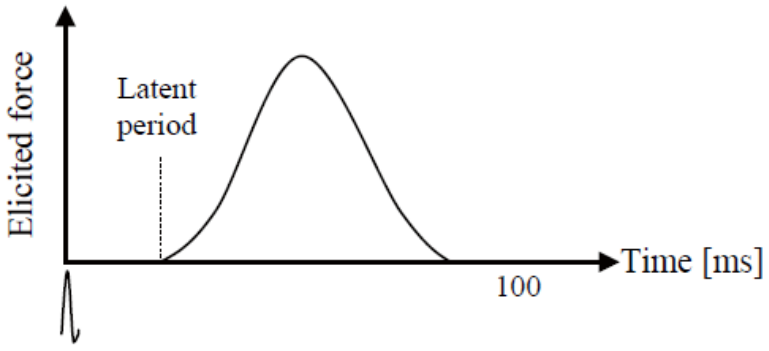

Figure 2.3: Response to a single stimulus as a result of a single twitch contraction, which may last 25-75 ms [2].

However, the stimulus amplitude is independent of the strength by which a muscle fiber responds to that stimulus (All-Or-None principle). Conversely, muscle strength is

associated to mechanical summation: as a result of higher stimulation regularity, the generated muscle force increases. Therefore, a sustained contraction (tetanus) results from a sequence of AP [2].

The overall resultant muscular contraction strength hinges upon the number of MUs recruited, as well as on the firing rate of the already recruited Motor Units (typically between 8 Hz to 35 Hz). Furthermore, according to the Henneman size principle, Motor Units are recruited according to their size in a voluntary contraction (first are recruited smaller MUs, being progressively larger MUs recruited with increasing muscle force) [2, 36, 37].

2.1.3 Electromyography (EMG)

The EMG signal is a biomedical signal which measures electrical potentials related to ionic currents (electrical activity of the muscle cell membrane) generated during muscle contraction. It represents neuromuscular activities and reflects the linear propagation of APs along the muscle fibers, depending as well from the anatomical and physiological properties of the muscles [2, 35]. The spatial and temporal algebraic sum of potential contributions from the active Motor Units can be acquired with electrodes, which measure an electric difference of potential as a function of time, due to the property of superposition of electric fields [34, 3]. These electrodes may be needle electrodes invasively inserted directly into the target muscle tissues (which measure a single fiber or a small number of fibers APs), or surface electrodes (non-invasive), attached to the skin surface (which measure the overall effects of the AP generated in the muscle fibers underlying the skin) [25, 2, 35].

Since electrical activity is affected by alterations in the MU's structure, EMG is often used as a diagnostic tool [26]. sEMG will be used in this work. Complexity, randomness, nonstationarity (statistical proprieties change over the time) and nonlinearity (muscle activity and EMG signal pattern don't exhibit a linear relationship) are some of the main characteristics of the sEMG signal [25]. Therefore, this signal presents a complex nature, with both structured (i. e. Motor Unit Action Potentials) and random-like (i. e. neural innervation) contributions [23].

The EMG signal strongly depends on the electrodes placement, since when incorrectly positioned, neighboring muscles' electric activity may influence the recorded signal (cross-talk) [2, 37]. The signal-to-noise ratio (ratio between the energy in the EMG signal and the energy in the noise signal) can also influence the signal's reliability. Hence, a higher ratio is concomitant with a better signal. The EMG signal's quality is influenced by the common mode rejection ratio as well, being a higher ratio associated to a better signal. Thereby, common interferences (e. g. from electric networks or distance from muscles) are rejected through differentiation [2, 35].

2.2 Technical base

2.2.1 Signal acquisition

The EMG signal is recorded using a bioPLUXresearch unit. Four pairs of electrodes are placed along the muscles, and data is collected by ipsilateral (electrodes positioned on the same side of the body) and contralateral (electrodes positioned on opposite sides of the body) acquisitions, while subjects perform a specific task. However, only ipsilateral analysis is executed (data collected from each arm of a subject will be analyzed separately). Data is collected from the first dorsal interosseus and extensor digitorum from each side of the body.

The device has eight analog channels with 12-bit resolution and also an external channel to be used as a reference ground, and is used a sampling frequency of 1000 Hz. To ensure there is no loss of information, sampling frequency must be at least twice the signal's maximum frequency (Nyquist sampling theorem) [34, 38].

2.2.2 Low-level signal processing

The sEMG analogue signal (continuous in time) has to be converted into a discrete digital signal and analyzed both in time and frequency domains. Hence, the signal is usually rectified (the signal is transformed into its absolute value) and filtered (a specific range of frequencies will be attenuated and only the passage of the frequency of interest is allowed).

2.2.3 High-level signal processing

In order to characterize the sEMG signal, Coherence, PLF, FD, LZ, DFA and MSE methods, as well as a classification algorithm were used. These methods are described below.

2.2.3.1 Coherence

Neuronal synchrony can be analyzed by frequency analysis. Therefore, it is necessary to perform the cross-correlation in frequency domain between two distinct signals, being coherence the main linear dependence (correlation) measure in the frequency domain. However, this measure does not provide the two signals' direction of interaction (direct coherence) [17, 18, 39]. Considering two signals x and y (e. g. rectified and normalized EMG signals stationary zero mean time series) at frequency λ, coherence can be computed using auto-spectra – $f_{xx}(\lambda)$ and $f_{yy}(\lambda)$ – and cross-spectra – $f_{xy}(\lambda)$ – estimations by averaging discrete Fourier transforms of non-overlapping data segments taken from each signal. Eq. 2.1 expresses the coherence function, $|R_{xy}(\lambda)|^2$, defined as the absolute square of the cross-spectrum normalized by the product of each signal's auto-spectra [19, 17, 39].

$$|R_{xy}(\lambda)|^2 = \frac{|f_{xy}(\lambda)|^2}{f_{xx}(\lambda)f_{yy}(\lambda)} \tag{2.1}$$

Coherence function estimates values from 0 to 1, assuming the value 0 if there is no association between the two signals at that frequency, and the value 1 if there is a perfectly linear association between them [19, 17, 39]. The strength and range of frequencies of common rhythmic synaptic inputs dispersed across a motoneuron pool may be quantified with coherence estimations [19].

2.2.3.2 Phase Locking Factor (PLF)

PLF is a measure of synchronization between two signals. Considering oscillatory time series, it is possible to obtain meaningful phase values, which can be used as synchronization indicators. The EMG signal, as the majority set of measurements available from real-world applications, assumes real values. However, in order to analyze a signal's phase, it is suitable to convert the real-valued signal into a set of complex-valued data. Therefore, it is required the application of a transformation to extract the rotation angle over the time by projecting the time series onto a circumference [40, 41, 42].

Before the phase reconstruction procedure (which is only valid if the signal comprises a clear oscillatory component), the presence of oscillatory activity may be assessed through the observation of significant values in the power spectrum. The frequencies of interest are then isolated by the application of a band-passed filter at a narrow band centered at each frequency. It is obtained an oscillatory signal from which the phase, or rotation angle, can be defined in the complex unit circle. In this work the method used to perform this task is based on the application of the Hilbert transform. Phase correlations between signals can then be studied, and correlation indices (e. g. phase coherence) can be computed in order to evaluate the strength of phase locking between two signals. The number of oscillation cycles considered influences this analysis. For a stationary time series, more oscillatory cycles (i. e. longer observation times) provide more reliable estimates while shorter observation times may lead to the concealment of important interactions (e. g. if they are weak or masked by noise). For a nonstationary time series, long observation times may not capture the presence of transient interactions [40].

Given two signals j and k, with phases $\phi_j(t)$ and $\phi_k(t)$ respectively, for $t = 1, \ldots, T$ (being T the number of discrete samples, i. e. the observation period), PLF between these two signals is defined by eq. 2.2 [41, 42]:

$$\rho_{jk} \equiv |\frac{1}{T}\sum_{t=1}^{T} e^{i[\phi_j(t)-\phi_k(t)]}| = |\langle e^{i[\phi_j(t)-\phi_k(t)]}\rangle| \tag{2.2}$$

PLF ranges from 0 to 1. While $\rho_{jk} = 0$ corresponds to asynchronous signals (their phases are not correlated), $\rho_{jk} = 1$ is attained if the two signals are in perfect synchronization (their phase lag is constant), for an observation period sufficiently long. Partial synchrony is obtained for PLF values between 0 and 1. In other words, PLF evaluates if

the two signals' phase difference is strongly or weakly clustered around some angle in the complex unitary circle [41, 42].

In this work, PLF between two signals will be calculated for moments of steady contraction, where oscillations are expected.

2.2.3.3 Fractal Dimension (FD)

Fractal dimension's concept arose from the need of a quantity other than length to distinguish numerous degrees of complication for a geographical (statistically self-similar) curve, as described in [43] by *B. B. Mandelbrot*. When a straight ruler is used to measure a country's coastline, different estimates of its dimension are obtained according to the scale applied to the ruler, i. e., according to the ruler's resolution. In other words, smaller rulers (higher resolutions) provide larger coastline measures. Hence, the concept of length becomes meaningless for geographical curves [43]. FD is then used, for instance, to describe an object extremely detailed to be one-dimensional, whereas too simple to be two-dimensional.

EMG, Electroencephalogram (EEG) and Electrocardiogram (ECG) are complex medical biosignals in which small scale structures (signal patterns) exhibit self-similarity with larger scale structures. This self-similarity phenomenon, which occurs with fractal scale relationship, can be described as the scale invariance of a process, and can be determined by the application of FD [20, 21, 44]. In other words, fractal objects resemble each other independently of the visualization scale or magnification. Altering the measurement scale and measuring changes in the curve's length allows an estimation of the FD [20]. These fractals properties are expected to be found in a sEMG signal since the source of the sEMG recordings are similar APs [20].

Despite the existence of multiple definitions for FD, such as Hausdorff dimension, correlation dimension, Higuchi dimension, box dimension, information dimension, among others, they are usually characterized by a non–integer fractional number [21, 25, 44].

It is documented in literature [21, 22] that FD for physiological signals is more accurately estimated using Higuchi algorithm for non-periodic and irregular time series. In case of small number of data, this algorithm gives a reasonable estimation of FD [25]. The Higuchi method has been successfully tested with the upper-limbs movement [25].

In order to apply the Higuchi method, it is firstly defined a new time series X_k^m from a signal sampled at a fixed sampling rate, $x(n) = X(1), X(2), X(3), \ldots, X(N)$, as showed in eq. 2.3 [21, 25, 22]:

$$X(m), X(m+k), X(m+2k), \ldots, X(m+\lfloor(\frac{N-m}{k})\rfloor \cdot k) \quad \text{and} \quad m = 1, 2, ..., k \tag{2.3}$$

Where m represents the initial time and k the interval time, and they are both integers. Then the length of the curve X_k^m is determined accordingly eq. 2.4 [20, 21, 25, 22]:

$$L_m(k) = \frac{[\sum_{i=1}^{\lfloor N-\frac{m}{k} \rfloor} |X(m+ik) - X(m+(i-1)k)|] \frac{(N-1)}{\lfloor \frac{(N-m)}{k} \rfloor \cdot k}}{k} \tag{2.4}$$

Where $\lfloor\rfloor$ denotes the Gauss' notation. The average value over k sets of $L_m(k)$ is the curve's length for the time interval k, $\langle L(k) \rangle$. The curve is fractal with the dimension D if $\langle L(k) \propto k^{-D} \rangle$. Afterwards, the linear relationship between $L(k)$ and k is plotted in a log-log graph, and an FD estimation for a statistical self-similar curve can be obtained from the slope of the plotted line [21, 25, 22].

As previously referred, another definitions of FD may be used, however they will not be described in this work.

Another important feature is Maximum Fractal Length (MFL), which is the signal's length (over unit time) measured from the logarithmic plot determining FD at the smallest scale. MFL value is significantly influenced by singularities originated from the proximal muscles, since background activity has smaller magnitudes and for this reason doesn't influence MFL so greatly. Since the density of singularities within a signal is related to MFL, this feature indicates the Motor Unit Action Potentials (MUAPs) rate in a sEMG signal, which is a more direct measure of the relative strength of muscle contraction [21, 22].

2.2.3.4 Lempel-ziv (LZ)

The LZ complexity measure can be used to analyze the deterministic complexity of a highly non-linear deterministic and chaotic setting [23]. In other words, this feature is used to evaluate finite sequences randomness and has been applied to evaluate the degree of complexity of biomedical signals, including EMG [24].

In order to compute the LZ measure, the sEMG signal, $x(i)$ (or any other discrete time signal of N samples) must be converted into a symbolic sequence, $s(i)$, conventionally a binary sequence, by comparison with a threshold. Thus, if the sEMG signal is smaller than that threshold, the signal takes value 0, otherwise, it takes value 1, which is mathematically expressed by eq. 2.5. Eq. 2.6 represents the symbolic sequence S [23, 24, 45].

$$s(i) = \begin{cases} 0, & \text{if } x(i) < \text{threshold} \\ 1, & \text{otherwise} \end{cases} \tag{2.5}$$

$$S = s(1), s(2), ..., s(n) \tag{2.6}$$

Afterwards, it is determined the number of different patterns P contained in the sequence S. In order to do that, it is necessary to denote [23, 24]:

1. The length of the symbolic sequence S: N

2. The integer number of different symbols of a finite alphabet in which the original

sequence is converted: β (for a binary sequence $\beta = 2$)

3. A collection (designated as vocabulary) of all of the substrings that belong to the sequence S: $v(S)$
4. Two distinct substrings of the sequence S: $Q = s_1, s_2, \ldots, s_q$ and $R = s_{q+1}, s_{q+2}, \ldots, s_{q+r}$
5. A concatenation of the substrings Q and R: $QR = s_1, s_2, \ldots, s_{q+r}$
6. A substring of the sequence S derived from QR after the removal of its last character: $QR\pi = s_1, s_2, \ldots, s_{q+r-1}$

The scanning process begins with the initialization of the sequences S, R and P ($S = s_1$, $R = s_2$ and $P = 1$), being the symbol s_1 the first pattern. Afterwards, it is added to the substring R a new subsequent element, s_i, of the sequence S until R doesn't belong to $v(QR\pi)$. Hence, if the sequence R doesn't belong to $v(QR\pi)$, R is defined as a new distinct pattern of the sequence S and the sequence P is increased by one. Then, Q and R are reset ($Q = QR$ and R takes the value of the subsequent element s_i of S) for the next iteration. This process continues until $QR = S$ [23, 24].

For example, applying this method in a binary sequence (with two symbols, $0, 1$, $\beta = 2$) $1, 0, 1, 1, 1, 0, 1, 0$, it would be obtained the parsed sequence $1.0.11.10.10$, where distinct patterns are separated by a period. In this example $P = 4$ [23].

Finally, after P has been found, this sequence is normalized by the number of characters β and the length, N, of the sequence S, as expressed by eq. 2.7, being C_β the normalized LZ complexity value of S [23, 24].

$$C_\beta = \frac{P \log_\beta(N)}{N} \tag{2.7}$$

In this work will be used a binary sequence.

2.2.3.5 Detrended Fluctuation Analysis (DFA)

Detrended Fluctuation Analysis is frequently used as a nonlinear analysis method or a fractal time series algorithm, being typically applied to noisy signals, since it is an important tool in the detection of long range correlations. This is a very advantageous method, since it combines the advantages of both time domain and time-frequency domain features. DFA also outperforms spectral analysis features, such as Discrete Wavelet Transform and Wavelet Packet Transform [25].

The DFA method can be applied to the study of electrophysiological signals, being a modified Root Mean Square (RMS) analysis of a random walk. In order to describe this method's procedure it is necessary to denote $\{x(t)\}$ as the sEMG time series, being t the discrete time in the range $[1, N]$ (N is the time series' sample length) [25].

First the sEMG signal is integrated in order to be converted into random walk. Eq. 2.8 expresses this integrated series (also known as profile or cumulative sum $y(k)$), being $\overline{x(t)}$ the average value of $x(t)$ [25]:

$$y(k) = \sum_{t=1}^{k} [\{x(t)\} - \overline{x(t)}], \quad k = 1, ..., N \tag{2.8}$$

Then these integrated series are parted into L identical windows (box sizes) and each window has an n time point. This point, n, is a DFA parameter, and it is the largest integer smaller than N divided by L [25].

Afterwards, a least-square fit is applied to the integrated series $\{y(k)\}$ within each window, being each window's least-square line the semi-local trend within that window. This is another DFA parameter. After this, the integrated series and the detrended time series RMS fluctuation is computed. This is given by eq. 2.9, where $y_n(k)$ is the y coordinate coefficient [25]:

$$F(n) = \sqrt{\frac{1}{N} \sum_{k=1}^{N} [y(k) - y_n(k)]^2} \tag{2.9}$$

Finally, this calculations are repeated for every window, in order to obtain the log-log graph of the linear relationship between $F(n)$ and n. The common base 10 logarithm is applied, and the fluctuation showed in the graph is characterized by the slope of the line which relates $\log F(n)$ to $\log n$. This slope is the DFA's scaling exponent α which is the power law (fractal) scaling. α is a self-similarity parameter and is given by eq. 2.10 [25]:

$$\alpha = \frac{[\Delta \log_{10}(F(n))]}{[\Delta \log_{10}(n)]} \tag{2.10}$$

The DFA's scaling exponents assume values between 0 and 2. According to its value the time series behavior can be explained. Therefore:

- If $0 < \alpha < \frac{1}{2}$ the time series is anti-correlated
- If $\alpha \cong \frac{1}{2}$ the time series is uncorrelated, or indicates white noise (the value at one instant cannot be correlated with any previous value)
- If $\frac{1}{2} < \alpha < 1$ the time series is correlated
- If $\alpha \cong 1$ indicates pink noise ($\frac{1}{f}$ noise)
- If $1 < \alpha < \frac{3}{2}$ indicates nonstationary or random walk
- If $\alpha \cong \frac{3}{2}$ indicates Brownian noise (i. e. the integration of the white noise)

This value is related to the FD parameters by a linear relationship, since larger scale exponent α values correspond to smaller FD [25].

An optimal exponent of the DFA method is dependent of the window function, the order of the fitting procedure and the sample length, N, of the feature. Therefore, it is important to do a well adjustment of these parameters [25].

The window function depends on the maximum and minimum window size and the function's increment interval. In literature [25] are proposed experiment suggestions for the first two parameters. The adjacent interval can be defined as an arithmetic progression or as a geometric progression. For the fitting procedure, different types of polynomial fits can be used (linear, quadratic, cubic and so on).

2.2.3.6 Multiscale Entropy (MSE)

Entropy has been often used to quantify complexity, since traditional entropy definitions (e. g. Shannon-entropy) are used to measure disorder and uncertainty, as well as to characterize a systems' gain of information [28]. Approximate Entropy and its modification Sample Entropy are entropy-based complexity measures with a single scale which are widely used in short and noisy time series. Based on these two features, Multiscale Entropy (MSE) has been introduced [27, 28, 46].

In order to compute the Sample Entropy it is necessary to denote:

1. The time series $x(i) = \{x_i, x_{i+1}, x_{i+2}, \ldots, x_N\}$ of length N [27, 28, 46];
2. Two m-dimensional sequence vectors, $y^{(m)}(i) = \{x_i, x_{i+1}, x_{i+2}, \ldots, x_{i+m-1}\}$ and $y^{(m)}(j) = \{x_j, x_{j+1}, x_{j+2}, \ldots, x_{j+m-1}\}$. These vectors are embedded from the time series $x(i)$ in a delayed m-dimensional space. They are considered similar (i. e. they match) if their distance is smaller than a tolerance r [27, 28];
3. The probability (density) $\rho^m(r)$ of two vectors match in the m-dimensional space, which is calculated by counting the matched vector pairs' average number. This probability is also computed for the embedded dimension $m+1$, in order to estimate $\rho^{m+1}(r)$ [27].

Therefore, Sample Entropy is defined according to eq. 2.11:

$$SampEn(m, r) = \log[\frac{\rho^m(r)}{\rho^{m+1}(r)}] \tag{2.11}$$

In order to obtain the MSE, the simple "coarse-grained" multiscale approach is applied on the original time series, $x(i)$, before the entropy measure. $x(i)$ is then segmented into $\frac{N}{\tau}$ coarse-grained sequences with length τ, and the mean value is calculated for each segment. Eq. 2.12 shows the new coarse-grained time series, $\{v_j(\tau)\}$, where $\tau = 1, 2, 3, \ldots$ [27, 28].

$$v_j(\tau) = \frac{1}{\tau} \sum_{i=(j-1)\tau+1}^{j\tau} x_i, \quad 1 \leq j \leq \frac{N}{\tau} \tag{2.12}$$

Then, Sample Entropy is computed over these multiple scales (m-dimensional vectors $y^{(m)}(i, \tau)$ are built from this new time series as previously illustrated). Hence, MSE is a variation of the Sample Entropy as a function of τ, the scale factor. The coarse grained

approach introduces linear smoothing (the high frequency components are gradually removed of the original time scale) and decorrelation between the vectors [27, 28, 46]. Furthermore, Entropy decreases with the scale factor concerning White noise, remaining constant for all scales regarding $1/f$ noise (correlated fluctuations), which is consistent with the fact that $1/f$ noise is more complex than White noise [47].

The two free parameters m (the sequence length) and r (the tolerance level) are associated with the likelihood of two sequences of length m stay close to one another at the next step within a certain tolerance level r. Consecutive sequences are identical when the output is zero. Decreasing the tolerance level will increase the entropy value, since it will be harder to find consecutive sequences close together within the given tolerance level. Therefore, both of the parameters aren't absolute measures [28]. In literature [28] it is proposed to use $m = 2$ and $r = 0{,}15\sigma$, being σ the standard deviation of the original time series.

It is important to reference that in the multiscale approach, increasing the value of τ will decrease the data variation. Also, the tolerance value is assumed to be the same for all scales (the standard deviation value is not adjusted for each scale), reason why the standard deviation value of a given data set diminishes when τ increases. However, it doesn't exist a general relationship between standard deviation and the entropy, being that relationship dependent of the correlation properties [28].

2.2.4 Classification

Classification methods are used in order to identify the belonging of a novel observation in a set of categories (sub-populations). These categories are obtained with basis in a training group of observations. It is necessary to have previous knowledge of the category membership of each observation of the training group. These observations are then analyzed in various levels, according to the used features (quantifiable properties). In this project, the used features are: kurtosis, maximum frequency, mean, median frequency, power band, spectral kurtosis, spectral skewness, spectral spread and correlation. There will be also analyzed the results of the previously referred implemented algorithms (coherence, PLF, FD, LZ, DFA and MSE). Classification can be implemented throughout a various number of algorithms, the classifiers, described below. Leave-one-out cross validation iterator is used to split data in train/test sets. Hence, all samples except one are used as a train set, being this left out sample tested after [48].

2.2.4.1 k - Nearest Neighbors

The k-Nearest Neighbors technique consists in the attribution of a certain point into the dominant class according to its distance to the nearest neighbor(s) within the training group. This distance can be, generally, any metric measure, being the Euclidian distance normally used [48, 49].

2.2.4.2 Decision Tree

A Decision Tree is a hierarchical tree structure based on a series of rules concerning the attribution of classes to the input sample data. This structure consists of a root node, internal and external nodes, connected by branches. Each internal node (nonleaf node) is concomitant with a decision function in order to determine the following node, splitting the value into different branches corresponding to different attributes, whereas each external node (leaf node) denotes a class. Generally, the Decision Tree algorithms procedure consists in two steps: tree building and tree pruning [50, 32].

2.2.4.3 Random Forest

The Random Forest algorithm is applied to K samples drawn with replacement from the training group (bootstrap samples). Then, unpruned regression trees are built for each bootstrap sample. When splitting a node during this tree construction, it is chosen the best split among a random subset of features (i. e., the algorithm randomly samples p_0 ($0 < p_0 < p$) of the p predictors (input variables)), instead of the best split among all the predictors. Finally, the predictions of the K trees are averaged, in order to predict new data [48, 33].

2.2.4.4 AdaBoost

The AdaBoost method uses a linear combination (ensemble) of several weak classifiers (simple decision rules) which when combined originate a strong classifier (decision rule more complex and accurate). This sequence of weak classifiers is applied to repeatedly modified versions of the data set. These modifications consist in the application of weights ($w_i = w_1, w_2, \ldots w_N$) to each sample of the training group. In the first iteration the weak classifier trains on the original data set (all the weights are initially set to $w_i = \frac{1}{N}$). The data set is reweighted for each successive iteration: the weights of incorrectly predicted training examples at previous iterations increase, while the weights of correctly predicted training examples decrease. Hence, the subsequent weak classifier is obliged to focus on the missed examples of the previous weak classifier [48, 29].

2.2.4.5 Naïve Bayes

The Naïve Bayes technique is based on the application of the Bayes theorem with the naïve presupposition that every pair of features is independent. Defining y as a class variable and $x_i = x_1, \ldots, x_n$ as a dependent feature vector, the classification rule defined by $\hat{y} = \arg\max_y P(y) \prod_{i=1}^{n} P(x_i|y)$ can be followed. Therefore, the maximum a posteriori estimation can be used to estimate $P(y)$ and $P(x_1|y)$ [48].

3

Acquisition Methods

3.1 Subjects

Contralateral and ipsilateral measurements were simultaneously performed in two different groups of subjects: a group of patients presenting ALS and a group of control, which members do not show any evidence of a known neuronal or muscular disease, except one member who is diagnosed with Kennedy disease. The ALS onset form is also different among the group of patients: Bulbar (B), Left lower limb (LLL), Right lower limb (RLL), Right upper limb (LUL), Right Upper Limb (RUL), Upper limbs (UL) and axial. One member of patients group is diagnosed with Primary Lateral Sclerosis (PLS). Some of the patients presented motor difficulties, which restricted their own movement control. Hence, the sEMG signal acquired from some of them could not be analyzed, since moments of contraction could not be isolated. Within this assemblage, some patients acquired sEMG signal from only one arm, due to their inability of self-controlled movement, while others have acquired from both arms but the signal from one of them was impossible to process. Therefore, the patients group contains 21 subjects, varying this number according to the analyzed channel (left or right hand or forearm). The control group contains 26 subjects. All participants from the patients group have been diagnosed within less than three years, except one which was diagnosed 97 months ago, and the patient with PLS which was diagnosed 10 years ago. All the patients are medicated with Riluzole. All participants from both groups have ages between 23 and 77 years (mean of 58,9 years for the patient group and 45 years for the control group).

3.2 Acquisition Protocol

The performed task, visible in Figure 3.1, was repeated for 6 minutes or less according to maximum time borne by the patients. Subjects sat down and placed both hands and forearms on a desk in a parallel position, 10 cm away from each other with hand palms facing one another in 90 degrees flexion with the elbow. While listening to a programmed sound, which guided the movement, subjects were asked to coordinately elevate both index fingers vertically with maximum articular amplitude in an opposite direction from the other fingers position, hold that position for 3 seconds while maintaining a certain force and return to the original position, remaining in that position for 3 seconds while trying to relax the arms muscles as much as possible.

3.3 Recording

As previously stated, contralateral and ipsilateral acquisitions were recorded simultaneously, and 4 signals were acquired from each subject (with the exceptions specified in section 3.1) using EMG sensors attached to a bioPlux device (device specifications explained in section 2.2.1). Each sensor has two connected electrodes. The sensors were placed on the first dorsal interosseus muscle for both left and right hand, and on the extensor digitorum communis muscle for both left and right forearm. Ground was placed on ulna bone inferior extremity, where no muscle activity is present. Figure 3.1 shows the surface electrodes placements. Trying to better isolate moments of contraction, two accelerometer sensors were placed in the index finger, being acquired two signals for the z axis, one for the left and another for the right hand. These signals were only acquired for some subjects from the patient and the control groups, since this procedure did not demonstrate to be efficient.

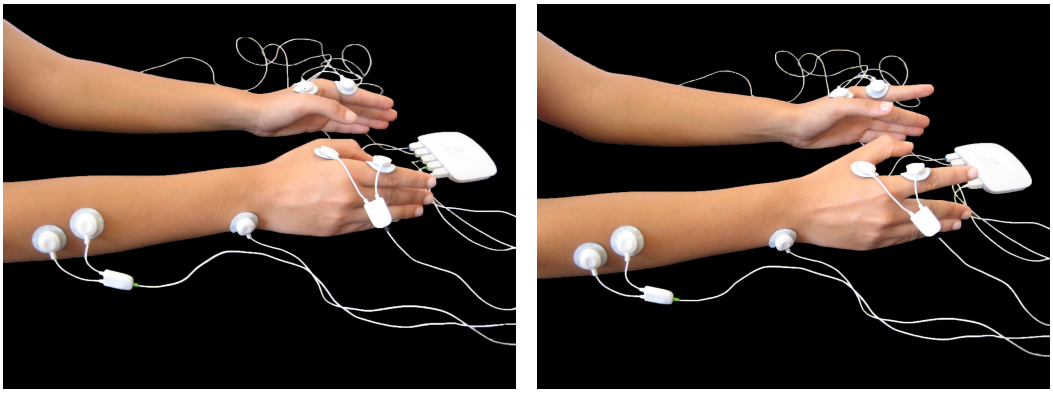

(a) (b)

Figure 3.1: Simultaneous contralateral and ipsilateral experimental setup: Bioplux research device, placement of four EMG sensors and ground. (a) Instant of relaxation. (b) Instant of contraction.

4

Signals Processing

4.1 Low-level Processing

All acquired signals were processed using python language. First, the signals' amplitude was converted from 'bins' into 'mV' and its Direct Current Component (DC) was removed. Then, it was applied a third order butter band pass filter of 10 – 500 Hz. From each pair of ipsilateral signals, intervals of common contraction were isolated from intervals of relaxation. It is not possible to predefine a common onset value to all signals due to the differences among each subjects' signals, as well as the different amount of noise inherent to each one of the signals. The used algorithm is explained in [51]. From this algorithm result an onset (beginning of an activation) and an offset (ending of an activation) for each contraction, which is different among the signals collected from the left and from the right arms. However, since the analysis is made for ipsilateral acquisitions, and assuming that subjects performed the task properly, without exerting any unrelated contractions regarding the task, it is possible to find the onset values for the hand and use those same values for the forearm as well.

4.2 High-level Processing

All of the algorithms were applied to moments of contraction. While coherence and PLF were calculated twice for each subject, being calculated for a pair of signals, FD, LZ, DFA and MSE were calculated four times, being applied to each one of the four acquired signals individually. Coherence and PLF were calculated for two common sections of data from an interval of one contraction. This was performed for all contractions, with

posterior averaging of all epochs. FD, LZ, DFA and MSE calculus was applied to a concatenation of all contractions.

4.2.1 Coherence Processing

Prior to coherence calculus, all EMG signals were full-wave rectified and then, for each contraction, coherence was calculated using matplotlib.mlab.cohere tool. Coherence is then calculated for an average of these moments of contraction. The used sampling frequency is 1000 Hz, the NFFT is 512 and the value that dictates the dependency between Fast Fourier Transform (FFT) windows is NFFT/2. NFFT values are related to frequency resolution, and more precision in frequency resolution is obtained for higher values of NFFT or lower values of sampling frequency. Therefore, for a sampling frequency of 1000 Hz, making NFFT as 512 yields a resolution of 1.95 Hz. For NFFT 4096, resolution would be 0.244. Coherence was averaged for each frequency among all the subjects within the same group. The following coherence tests were also made for a few members of both groups:

- For the same signal, compute coherence for the first 10, the first 20, the first 30, and so on, until the total length of the signal be achieved, in order to analyze the influence of the signal's length in coherence calculus.
- For the same signal, compute coherence for only 10 contractions, from 10 in 10 contractions, along the whole signal's length, in order to analyze coherence over time.
- For the same signal, compute coherence per contraction and per relaxation, in order to analyze coherence over time.
- Compute coherence for the concatenation of all contractions, to analyze coherence with higher NFFT values.
- Find the frequency associated to the maximum value of coherence for frequency band, in order to analyze variability among subjects within the same group.

4.2.2 PLF Processing

PLF algorithm used in this work was developed by *Mafalda Camara* in [51]. All signals were full-wave rectified and each signal was band pass filtered in order to remove all the other undesirable frequencies. The used filter was $[f-2, f+2]$, being f the analyzed frequency. Therefore, PLF calculus was performed as many times as the number of frequencies to analyze. For each pair of contractions, the Hilbert transform is applied to both signals, using scipy.signal tools. As a result of this operation, each section of data is now converted to its corresponding imaginary representation. Phase lag between both signals is then calculated for each contraction by finding each sample's angle and subtracting them. Euler's formula is then applied to each phase difference and averaged

for all instants within the same contraction, according to eq. 2.2. Hence, a different PLF value is obtained for each contraction of the analyzed signals and, in order to attain a final value for each subject, PLF was averaged among all contractions within the same acquisition. Finally, for each analyzed frequency, PLF was averaged among all members within each group, for the patient and the control groups.

PLF was also calculated for a time lag between both signals, in order to study the time lag, for each frequency, correspondent to the maximum PLF value. This study was made in two ways:

- For a time lag of 100, 200 and 500 points (1 point corresponds to 1 ms) for only one contraction from one member of the control group and one member of the patients group. This contraction had its full length minus its initial 50, 100 and 250 and its final 50, 100 and 250 points respectively.

- For a time lag of 200 points for the central window of only one contraction from one member of the control group and one member of the patients group. This window had 500 or 1000 points.

PLF was also calculated for one contraction from a member of both groups divided in 5 windows of 500 points (obtaining 5 values of PLF) or 2 windows of 1000 points (obtaining 2 values of PLF).

4.2.3 FD Processing

Concerning the calculus of FD, a new time series was defined from each signal, according to eq. 2.3, with k_{max} defined as 128, value suggested in literature [25]. Hence, k_{max} embedded time series with dimension m were obtained for each signal. Then, for each one of these k_{max} series, the length of the curve $L_m(k)$ was estimated according to eq. 2.4, being obtained m different curves lengths. An average of the curves lengths was made for each one of the m time series, resulting an array with length k_{max}. A log-log graph was plotted with the linear relationship between $L(k)$ and k. A linear regression is estimated using numpy.polyfit and numpy.poly1d tools, being the used signal's FD coefficient the resultant negative slope. An average of the linear relationship of base 10 logarithm of $L(k)$ for each value of k was estimated among all subjects within each group, in order to compare both populations. An average of the FD coefficient was also calculated for all members within each group.

4.2.4 LZ Processing

In LZ processing, as previously referred, β was defined as 2, resulting a binary sequence. The LZ coefficient was calculated three times for each signal, according to the obtained binary sequence:

1. The filtered used signal was converted into a binary sequence with threshold defined as 0.

2. The filtered used signal was rectified and converted into a binary sequence with threshold defined as 0.4.

3. The envelope of the rectified filtered used signal was converted into a binary sequence with threshold defined as 0.12.

The first value of the sequence S is added to the vocabulary and to the sequence Q, being this the first pattern. P is initialized as 1 and R is initialized as the second element of the sequence S. At each iteration the subsequent symbol of S is added to R until R doesn't belong to the vocabulary. In that case, R is defined as a different pattern and P is increased by one. Q and R are then reset, being Q a concatenation between Q and R, and R the next subsequent element of S. This process stops when $QR = S$, and the LZ coefficient is then calculated according to eq. 2.7. Since this coefficient is greatly related to the number of different patterns within each signal, and the number of patterns is related to the length of the signal, all the signals were cut in accordance with the minimum reasonable signal length within both groups. Therefore, LZ coefficient was computed for the first 66164 samples of concatenated contractions of each signal (which corresponds to 66164 ms).

An average of the LZ coefficient was calculated for all members within the patients and the control's group.

4.2.5 DFA Processing

For DFA, the used signal was converted into an integrated series (or profile) according to eq. 2.8. Then a progression is constructed starting with $Minbox = 4$. Maxbox was defined as $N/10$, as suggested in literature [25], being N the number of samples of the signal. Two different progressions were constructed:

1. A geometric progression, GP, $n_i = n_1 * r^{(i-1)}, \quad r = 2$.

2. An arithmetic progression, AP, $n_i = n_1 + (i-1)d, \quad d = 2$.

Each value, n_i, of the resultant progression corresponds to the windows length at each iteration, being the number of windows estimated by N/n_i. This number must be an integer, reason why the profile length may be smaller than the length of the original signal. At each iteration, a linear regression is estimated within each window, using numpy.polyfit and numpy.poly1d tools. All the resultant coefficients of the linear regressions among the entire signal are subtracted to the profile and squared, with posterior averaging within the profile length. A square root is then applied. This procedure is repeated as many times as the length of the used progression, as evinced in eq. 2.9. A log-log graph was plotted with the relationship between $F(n)$ and n. This curve is then

parted in three segments, and three linear regressions are estimated within each one of these segments. The third segment is always excluded, since its slope is almost zero, being only regarded the first and the second segments. The first segment is between point A and point B, the second segment between point B and point C, and the third segment between point C and point D. All these points are defined in the base 10 logarithm of the n array. Point A is always the index 0 point and point D is always the last point of the array. Point C can also be automatically estimated for each signal's $F(n)$ according to the slope of the third segment. This slope is successively calculated starting at point D in reverse order until the slope is 0.03. The corresponding point is then defined as point C. This point is always different for each $F(n)$. Four different division points were chosen, as described below:

1. Point B takes the value of the array's index 3 point and point C takes the value of the array's index 10 point.

2. Point B takes the value of the array's index 5 point and point C takes the value of the array's index 10 point.

3. Point B takes the value of the array's index 3 point and point C takes the automatically estimated value referred before.

4. Point B takes the value of the array's index 5 point and point C takes the automatically estimated value referred before.

Since several of the last points of $F(n)$ present an almost zero slope, and this slope is to be excluded, the constructed progressions include only 150 indexes, reducing significantly the computation time.

Finally, the slopes of segments one and two correspond to the coefficients α_1 and α_2, respectively. The presented results are obtained using an arithmetic progression, and the segments were defined according to the first enunciated case. An arithmetic progression was chosen since it presents a higher number of more approximated points than a geometric progression, which allows a better visualization of $F(n)$'s trend. The first enunciated case was chosen since it presents a better fit within each segment.

White, Pink and Brownian noise where also tested in this algorithm.

One of the signals of a control group member was also used to compute DFA for a very short signal with a *MATLAB* algorithm available on the internet [52]. The only alteration made to this algorithm was changing the base e logarithm for the base 10 logarithm, with purposes of results comparison. Only the $F(n)$ graphic was compared, and the results demonstrated to be very similar for both algorithms.

An average of the linear relationship of base 10 logarithm of $F(n)$ for each value of n was estimated among all subjects within each group, in order to compare both populations. An average of the DFA coefficients, α_1 and α_2 was also calculated for all members within each group.

4.2.6 MSE Processing

In the MSE algorithm, the used signal's mean was subtracted to the signal, and this result was divided by the signal's standard deviation. Following literature suggestion [28], m was defined as 2, r was defined as 0.15σ and τ was defined as 20.

A coarse-grained time series was constructed according to eq. 2.12, being obtained τ new different series. Sample Entropy was then computed τ times, as described next. As referred at section 2.2.3.6, two vectors, $y^{(m)}(i)$ and $y^{(m)}(j)$, are associated to each one of the τ scales. At each iteration, $|y^{(m)}(i) - y^{(m)}(j)| < \tau$ and $|y^{(m)}(i+1) - y^{(m)}(j+1)| < \tau$ were tested and, if fulfilled the conditions, the numerator, $\rho^m(r)$, was computed using eq. 2.11. Then $|y^{(m)}(i+2) - y^{(m)}(j+2)| < \tau$ was also tested, which being true allows the computation of the denominator, $\rho^{m+1}(r)$, defined in eq. 2.11. The base e logarithm was then applied to the quotient $\rho^m(r)/\rho^{m+1}(r)$, in accordance with eq. 2.11. This implemented method was based on [53].

White and Pink noise where also tested in this algorithm.

The Sample Entropy value for each scale (each τ) was plotted in a graph. An average of this Entropy for each τ was estimated among all subjects within each group, in order to compare both populations.

One of the signals of a control group member was also used to compute MSE with a *MATLAB* algorithm available on the internet [54]. This *MATLAB* algorithm was also converted into python language, in order to validate the results of the developed algorithm. The results were very similar for both *MATLAB* and the developed algorithm, being this comparison made through graphic observation.

4.3 Algorithm validation

4.3.1 Noise generation

White, Pink and Brownian noise were simulated in order to test some of the developed algorithms.

4.3.1.1 White noise

Two kinds of White noise were generated: Gaussian White noise and Uniform White noise. Gaussian White noise was produced by generating a random signal with "normal" (Gaussian) distribution of mean 0 and variance 1, using numpy.random.randn tool. This noise signal, with 300000 ms, was used to test the DFA function. Uniform White noise was produced by generating a random signal uniformly distributed within the interval $[-1.5, 1.5]$ with 80000 ms, using numpy.random.uniform tool. This noise was used to test the MSE algorithm.

4.3.1.2 Pink noise

A random signal uniformly distributed within the interval $[-1, 1]$ was generated using numpy.random.uniform tool. The discrete Fast Fourier Transform (FFT) of the signal was obtained using scipy.fftpack.fft tool, and the module was then applied. The Discrete Fourier Transform sample frequencies were obtained using scipy.fftpack.fftfreq tool. The signal's FFT was divided by the square root of each frequency, and then the Discrete Inverse Fourier Transform (IDFT) was applied using scipy.fftpack.ifft tool. This procedure generates Pink noise. This noise was used to test the DFA algorithm for a signal with 297000 ms and to test MSE algorithm for a signal with 80000 ms.

4.3.1.3 Brownian noise

Brownian noise was generated as described in [55]. Brownian motion is computed according to the equations 4.1, being $N(a, b; t1, t2)$ a normally distributed random variable with mean a and variance b. N is statistical independent on different time intervals.

$$X(0) = X_0, \quad X(t + dt) = X(t) + N(0, \delta^2 dt; t, t + dt) \tag{4.1}$$

δ was defined as 0.25, dt as 0.1 and $x(0)$ as 0. Brownian noise was generated using scipy.stats.norm.rvs tool. This noise was used to test the DFA algorithm for a signal with 300000 ms.

4.3.1.4 Synthetic signals

Synthetic signals were generated in order to validate some of the algorithms.

A pair of signals was generated in order to test PLF algorithm. These signals are generated using eq. 4.2. Coherence algorithm was tested using a pair of signals generated using eq. 4.3.

$$signal = A\cos(t \times 2\pi \times f + \phi(t)) \times mod(t) \tag{4.2}$$

$$signal = (A\sin(t \times 2\pi \times f) + k) \times n(t) \times mod(t) \tag{4.3}$$

where A is the amplitude of the signal, being defined as 1 for both signals; t is the duration time of the signal, in seconds, being defined as a sequence of integer numbers incremented by one unit divided by the sampling frequency, 1000 Hz; f is the signal frequency, placed at 15 Hz for eq. 4.2 and at 30 Hz for eq. 4.3; $\phi(t)$ is the signal phase, being defined as Uniform noise within the interval $[-0.17, 0.17]$ with length t for one of the signals and as $\pi/3 + t \times 0.1$ for the other; k is the signal's envelope, being defined as 3; $n(t)$ is Gaussian noise with mean 0 and variance 1 (this portion was multiplied by 0.1 in order to obtain a signal output with values comparable with the EMG signals magnitude); and $mod(t)$ is used to guarantee instants of contraction and relaxation of 3000 ms,

being defined as the rest of the division of t by 6 bigger than 3.

The signals were created with $t = 297s$, which corresponds to 49 contractions.

Figure 4.1 shows an example of both signals, applied to PLF algorithm and Figure 4.2 shows an example of one of the signals used to test the coherence computation.

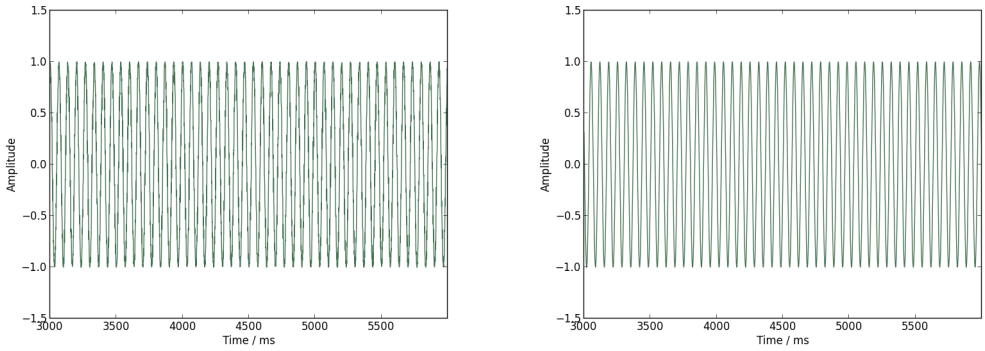

(a) (b)

Figure 4.1: Schematic representation of only 4 seconds of the 297 seconds (corresponding to 49 contractions) signal defined by eq. 4.2, with A defined as 1 and f placed at 15 Hz (a) Signal with $\phi(t)$ defined as Uniform noise. (b) Signal with $\phi(t)$ defined as $\pi/3 + t \times 0.1$

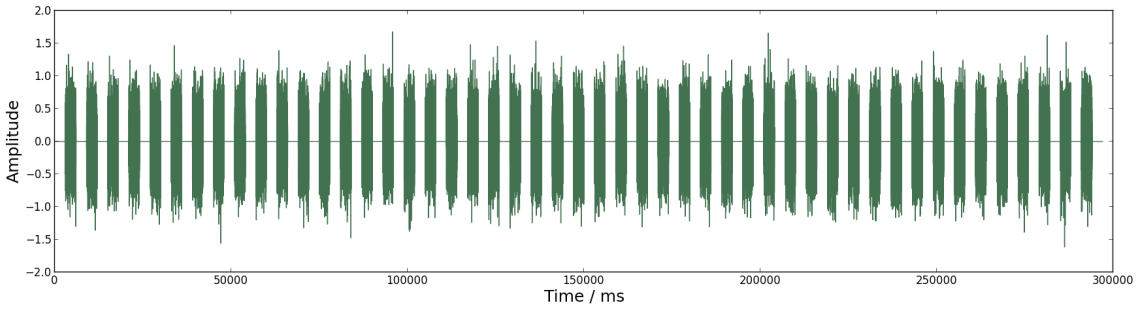

Figure 4.2: Schematic representation of the signal defined by eq. 4.3 with 297 seconds (corresponding to 49 contractions) with A defined as 1 and f placed at 30 Hz

Two random signals with 297 s were also generated using numpy.random.randn tool. Coherence between these two signals was calculated, as well as between one of the signals and itself.

4.4 Classification algorithm

The feature extraction and the classification algorithms were developed in another work, being available as a method for this work [56]. For further explanation consult [56]. The algorithms were adapted for the use of two channels, and the features extracted were selected according to this work objectives.

Features were extracted from a pair of signals (right hand and forearm). The sampling frequency was placed at 1000 Hz, being used a central window with 2000 points. The results obtained from the previously described algorithms were joined to these features.

Posteriorly several combinations of the extracted features, the developed algorithm results and of both of them were organized and classified with sklearn.neighbors.KNeigh--borsClassifier, sklearn.tree.DecisionTreeClassifier, sklearn.ensemble.RandomForestClas--sifier, sklearn.ensemble.AdaBoostClassifier and sklearn.naive_bayes.GaussianNB tools. The used cross-validation method was leave-one-out, from sklearn.cross_validation.Leave--OneOut.

5

Results and Discussion

5.1 Coherence Analysis

5.1.1 Coherence Tests

As previously referred in section 4.3.1.4, a pair of signals was created according to eq. 4.3, with $f = 30Hz$. Coherence was calculated for both signals and is presented at Figure 5.1. As expected coherence values are close to 1 for the specific frequency 30 Hz and near 0 for the remaining frequencies.

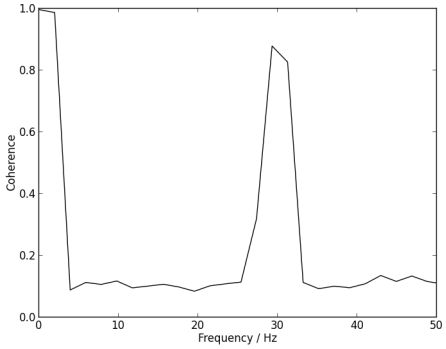

Figure 5.1: Coherence dependency on frequency for signals defined by eq. 4.3 with f as 30 Hz, using NFFT placed as 512.

Figure 5.2 represents coherence between a random signal and itself and two random signals. As expected, coherence assumes value 1 for all frequencies when calculated between a signal and itself, and very low values of coherence when calculated between two random signals.

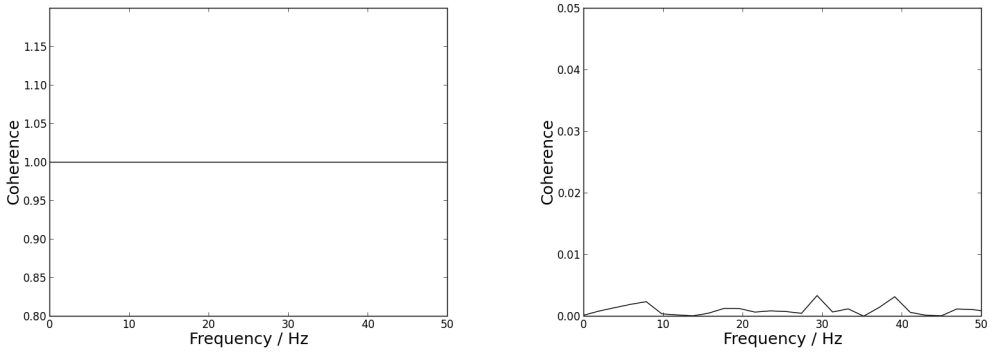

(a) (b)

Figure 5.2: Coherence dependency on frequency, using NFFT placed as 512. (a) Results for coherence calculated between a random signal and itself. (b) Results for coherence calculated between two random signals.

5.1.2 Coherence Results

Coherence mean values for the group of patients and for the control group are presented in Figure 5.3.

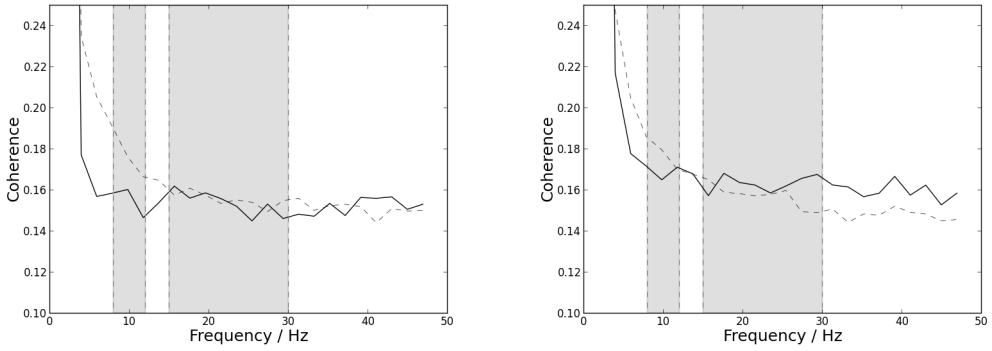

(a) (b)

Figure 5.3: Mean coherence dependency on frequency with NFFT placed as 512. Straight line for patients and dashed line for controls. The first grey box delimitates the frequencies corresponding to the alpha band ($8 - 12$ Hz). The second grey box delimitates the frequencies corresponding to the beta band ($15 - 30$ Hz). (a) Results from the left arm. (b) Results from the right arm.

By the observation of the graphics presented in Figure 5.3, coherence mean values are very similar for both the patients and the control groups. Control group mean value for coherence is slightly higher within the alpha band. Coherence pooled value for patients is $0,22 \pm 0,21$ for the left arm and $0,23 \pm 0,21$ for the right arm. Coherence pooled value for the control group is $0,22 \pm 0,21$ for the left arm and $0,22 \pm 0,21$ for the right arm. These values are different from those found in literature [14], since slightly higher values of coherence were expected for the control group within the beta band than for

the patients group. These differences may be explained by the sampling frequency used, differences in the acquisition protocol, differences in the used algorithm or parameters and the tested subjects themselves (age, gender, lifestyle, etc.). The obtained results are also different from the expected for ipsilateral acquisitions, since only preliminary results were obtained previously (comparison in coherence values for ipsilateral acquisitions was executed for only one member of each group in [51]).

Figures A.1 and A.2 of Appendix A present coherence mean and standard deviation values for the group of patients and the group of control, respectively.

In order to study the influence of the onset forms in coherence calculus, mean coherence among the subgroups of the patients group is presented in Figure 5.4.

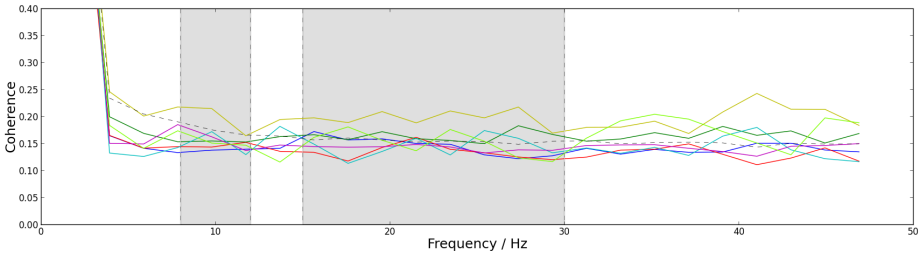

(a)

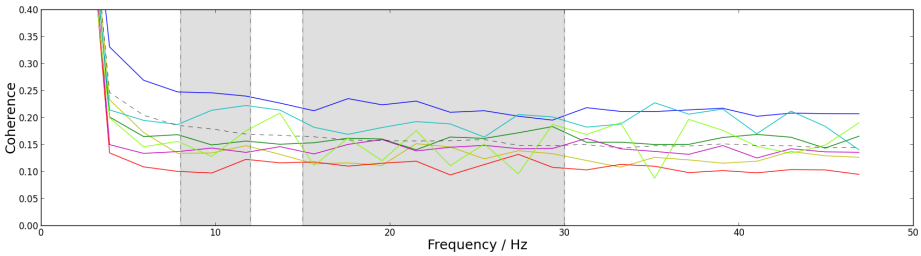

(b)

Figure 5.4: Mean coherence dependency on frequency with NFFT placed as 512. The dashed line represents the group of control and the straight lines represent the group of patients: yellow line is for onset form axial, dark blue line for B, red line for LLL, dark green line for LUL, light blue line for PLS, magenta line for RLL and light green line for UL. The first grey box delimitates the frequencies corresponding to the alpha band ($8 - 12$ Hz). The second grey box delimitates the frequencies corresponding to the beta band ($15 - 30$ Hz). (a) Results for the left arm. (b) Results for the right arm.

Observing Figure 5.4, the majority of the subgroups present smaller values for mean coherence for lower frequencies, except axial onset form for the left arm and B onset form, as well as PLS for the right arm. For higher frequencies, coherence mean values appear to be more similar among all the subgroups for the left arm than for the right arm, being the coherence mean values very similar to the control group as well.

Coherence was also studied for the same signal acquired for the same subject with different lengths and sections, as evidenced in section 4.2.1. Figures 5.5 and 5.6 present an example of these results for one member of each group for the right arm.

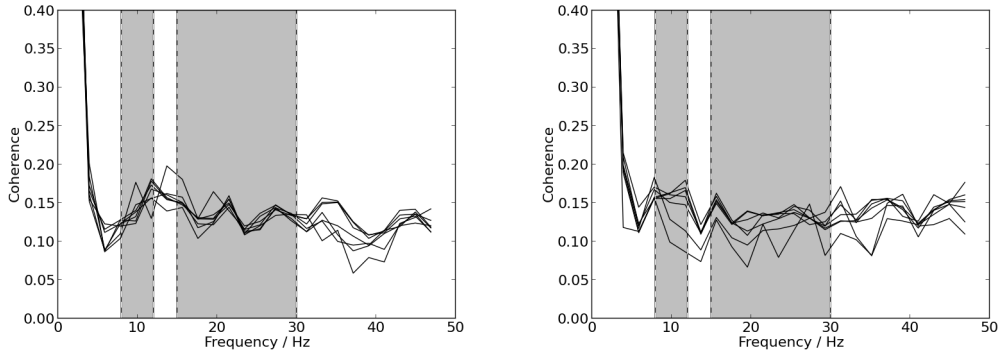

(a) (b)

Figure 5.5: Coherence values dependency on frequency for the right arm for different lengths of the same signal. The first grey box delimitates the frequencies corresponding to the alpha band ($8 - 12$ Hz). The second grey box delimitates the frequencies corresponding to the beta band ($15 - 30$ Hz). (a) Results for one member of the patients group. (b) Results for one member of the control group.

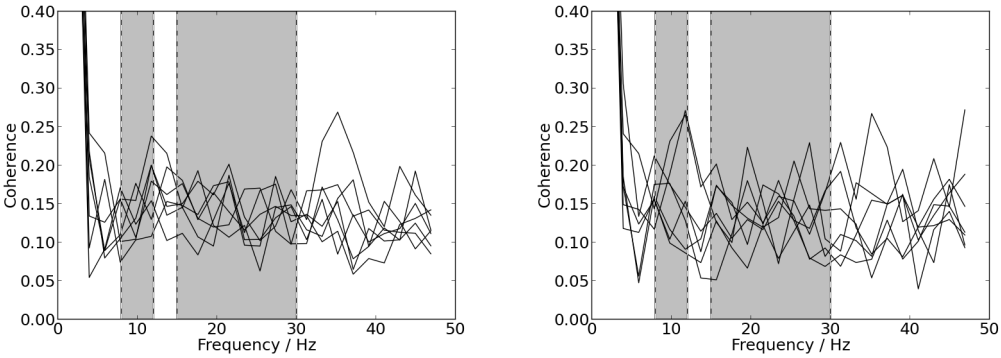

(a) (b)

Figure 5.6: Coherence values dependency on frequency for the right arm for ten different contractions of the same signal starting with the first ten until the last ten. The first grey box delimitates the frequencies corresponding to the alpha band ($8 - 12$ Hz). The second grey box delimitates the frequencies corresponding to the beta band ($15 - 30$ Hz). (a) Results for one member of the patients group. (b) Results for one member of the control group.

Figure 5.5 shows the same tendency for coherence independently of the signal length for both subjects, being the same peaks of coherence observed for the same frequency for almost all signals. Figure 5.6 shows a more dispersed coherence with the same peaks observed at a larger range of frequencies.

Coherence was also studied for each one of the existent contractions and relaxations of a signal. Figures 5.7 and 5.8 show an example of these results for one member of each group for the right arm.

Figures 5.7 and 5.8 show that coherence presents very distinct values according to

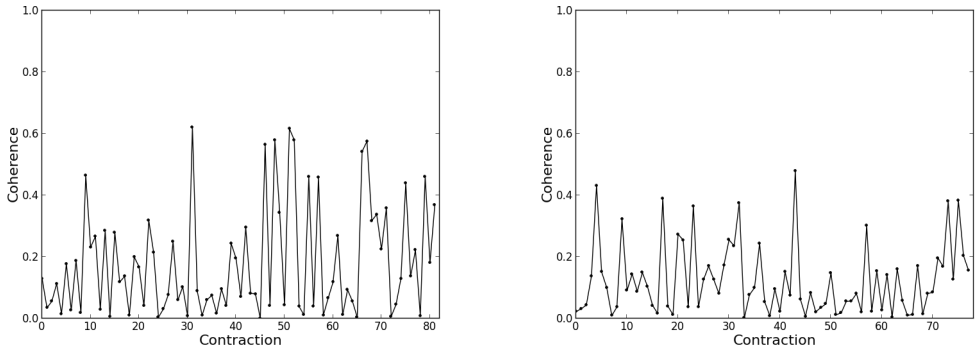

(a) (b)

Figure 5.7: Coherence values for each contraction for the right arm for frequency 17.58 Hz. (a) Results for one member of the patients group. (b) Results for one member of the control group.

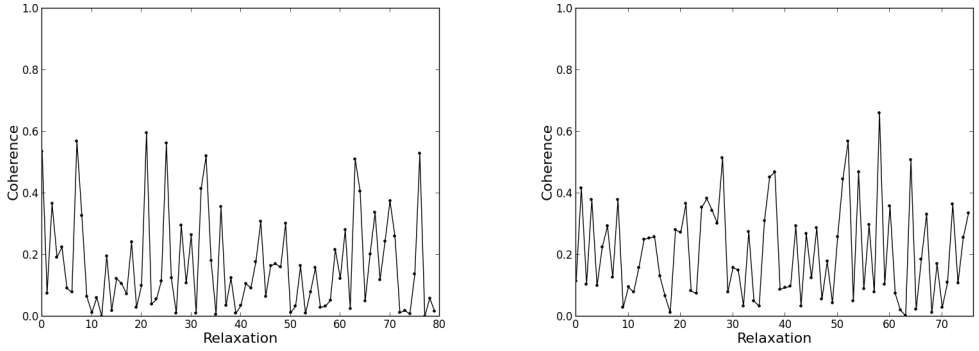

(a) (b)

Figure 5.8: Coherence values for each relaxation for the right arm for frequency 17.58 Hz. (a) Results for one member of the patients group. (b) Results for one member of the control group.

the contraction number, presenting values very close to zero with subsequent higher values for both subjects, which may explain the similar values of mean coherence obtained for both groups and presented in Figure 5.3. Coherence behavior for relaxation is very similar to contraction for this particular analysis.

Figure 5.9 represents maximum coherence for each frequency band (7 – 15 Hz, 15 – 22 Hz, 22 – 28 Hz, 28 – 36 Hz and 38 – 43 Hz) for patients and control groups for the right arm. By the observation of this figure, maximum coherence is not associated to a specific frequency, since all subjects among both groups present maximum coherence for different frequencies.

Figure 5.10 shows coherence mean values for patients and control group with coherence calculated for all the concatenated contractions with NFFT 4096. This graphic shows values of mean coherence lower than those obtained in Figure 5.3, which is expected

since coherence is computed along much longer signals, instead of being computed several times and posteriorly averaged. Coherence mean values are slightly higher for the control group than for the patients group within the alpha band (8 – 12 Hz).

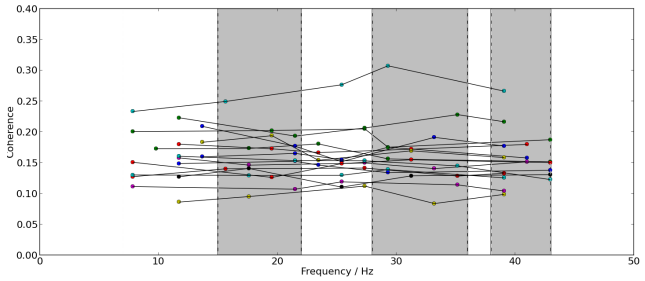

(a)

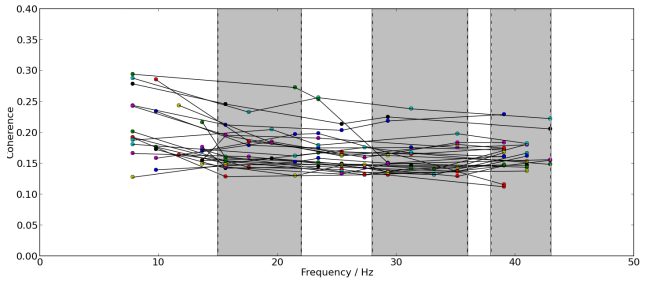

(b)

Figure 5.9: Maximum coherence values dependent on frequency for each member of patients and control groups for the right arm, with NFFT placed at 512. The grey boxes delimitates different frequency bands (from left to right, 15 – 22 Hz, 28 – 36 Hz and 38 – 43 Hz), being all the other frequencies represented by the white boxes. (a) Results for the group of patients. (b) Results for the group of control.

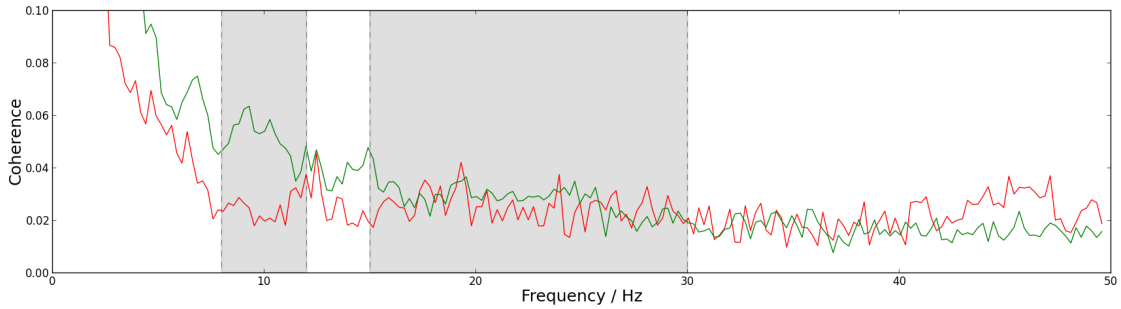

Figure 5.10: Mean coherence values dependency on frequency for the right arm, with NFFT placed at 4096. The used signals are a concatenation of all the contractions existent in each signal. The straight red line represents the patients group and the straight green line represents the control group. The first grey box delimitates the frequencies corresponding to the alpha band ($8 - 12$ Hz). The second grey box delimitates the frequencies corresponding to the beta band ($15 - 30$ Hz).

5.2 PLF Analysis

5.2.1 PLF Tests

As previously referred in section 4.3.1.4, a pair of signals was created according to eq. 4.2, with $f = 15Hz$. PLF was computed, being the results summarized in Table 5.1.

Table 5.1: Representation of the PLF mean and standard deviation values for the synthetic signals defined by eq. 4.2 with $A = 1$, $t = 297s$ and $f = 15Hz$.

Frequency / Hz	**5**	**10**	**15**	**16**	**17**	**18**	**19**
Mean PLF	0.37	0.23	0.20	0.21	0.24	0.28	0.33
Standard deviation	0.08	0.09	0.12	0.12	0.12	0.11	0.11
Frequency / Hz	**20**	**21**	**22**	**23**	**24**	**25**	**26**
Mean PLF	0.41	0.52	0.66	0.79	0.88	0.93	0.96
Standard deviation	0.10	0.09	0.07	0.05	0.03	0.03	0.01
Frequency / Hz	**27**	**28**	**29**	**30**	**40**	**50**	**100**
Mean PLF	0.97	0.98	0.98	0.97	0.31	0.14	0.20
Standard deviation	0.01	0.01	0.01	0.01	0.06	0.06	0.10

As evidenced in table 5.1, higher values of PLF, very close to 1, are presented for frequencies around 30 Hz. This is expected, since both signals are full-waved rectified before the PLF algorithm is applied. Since a cosine is being used, the frequency duplicates.

5.2.2 PLF Results

PLF mean values depending on frequency are presented in Figure 5.11 for both groups.

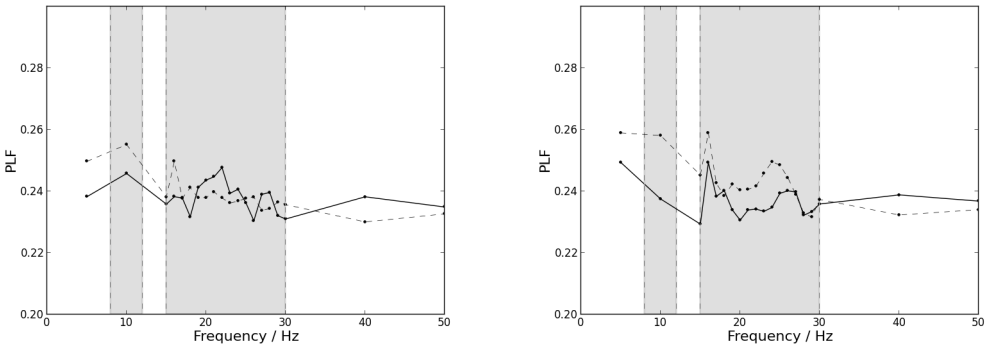

(a) (b)

Figure 5.11: PLF mean values dependency on frequency for patients by the straight line and for controls by the dashed line. The first grey box delimitates the frequencies corresponding to the alpha band ($8 - 12$ Hz). The second grey box delimitates the frequencies corresponding to the beta band ($15 - 30$ Hz). (a) Results from the left arm. (b) Results from the right arm.

Observing the graphics presented in Figure 5.11, PLF values appear to be very similar for both groups. Alpha band appears to demonstrate a higher difference between both groups' PLF values. However, since this work proceeds the investigation of PLF within the beta band [51], PLF was only computed for 10 Hz within the alpha band. PLF pooled value for the patients group is $0,238 \pm 0,005$ for the left arm and $0,237 \pm 0,006$ for the right arm. PLF pooled value for the control group is $0,239 \pm 0,007$ for the left arm and $0,242 \pm 0,009$ for the right arm. These results are very different from the obtained in [51], since a great distinction was expected between both groups. Differences in results may be explained by the length of the used signal, the sampling frequency used or the tested subjects themselves, since the comparison in PLF values for ipsilateral acquisitions was made for only one member of each group in [51], and characteristics such as age, gender and lifestyle may influence this analysis.

PLF mean values depending on frequency are presented in Figure A.3 of the Appendix A for the group of patients and in Figure A.4 of the Appendix A for the group of control.

PLF was also studied for a time lag between both signals for only one member of each group. This analysis was only executed for the right arm. An example of these results, for only two frequencies (17 Hz and 29 Hz) is presented in Figures 5.12, 5.13 and 5.14. The results for the other analyzed frequencies are similar. The obtained PLF values increase slightly for a certain time lag. However, it was not possible to define a consistent lag value. It is also possible to observe that PLF values calculated for smaller instants of contraction assume higher values.

Figure 5.15 shows an example of PLF calculated for one contraction from a member of both groups divided in 5 windows of 500 points, for the frequency of 17 Hz. The results for the other analyzed frequencies are similar, and PLF assumes maximum value for a different window within the contraction.

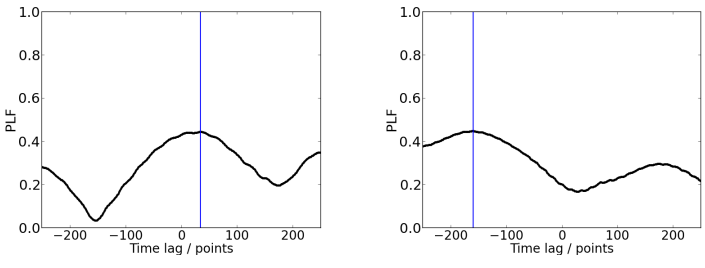

(a) (b)

Figure 5.12: PLF value for the right arm of the member of patients group calculated 500 times for one lagged contraction (time lag of 250 points to the left and 250 points to the right). A time lag of 500 points corresponds to 0.5 s. The blue vertical line indicates the maximum value of PLF. (a) Results for 17 Hz (PLF is 0.444 for point 34). (b) Results for 29 Hz (PLF is 0.448 for point -150).

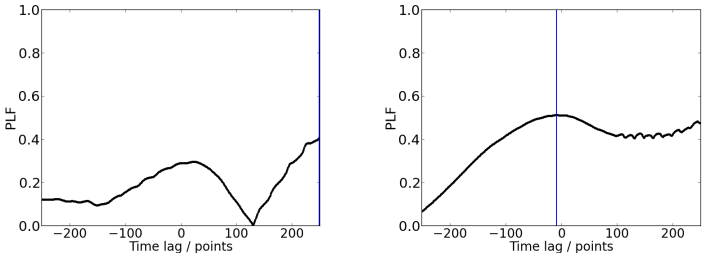

(a) (b)

Figure 5.13: PLF value for the right arm of the member of control group calculated 500 times for one lagged contraction (time lag of 250 points to the left and 250 points to the right). A time lag of 500 points corresponds to 0.5. The blue vertical line indicates the maximum value of PLF. (a) Results for 17 Hz (PLF is 0.409 for point 249). (b) Results for 29 Hz (PLF is 0.512 for point -9).

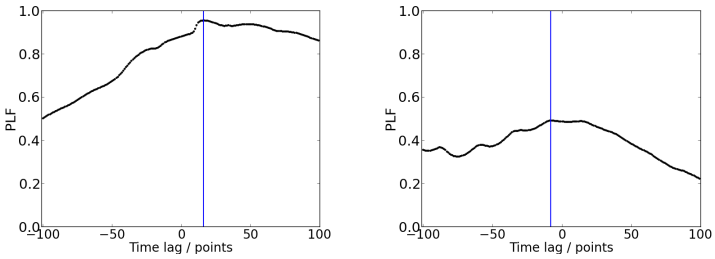

(a) (b)

Figure 5.14: PLF value for the right arm calculated 200 times for the central 500 points window of one lagged contraction (time lag of 100 points to the left and 100 points to the right). A time lag of 200 points corresponds to 0.2 s. The blue vertical line indicates the maximum value of PLF. (a) Results for 17 Hz for the member of the patient group (PLF is 0.956 for point 16). (b) Results for 17 Hz for the member of the control group (PLF is 0.493 for point -8).

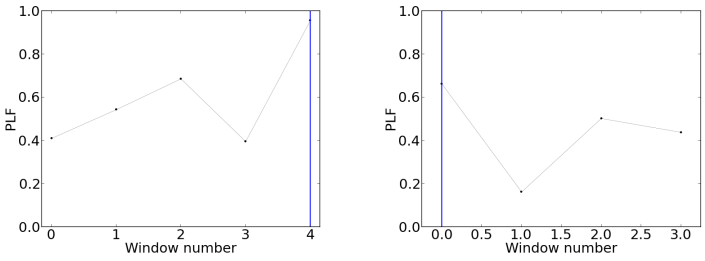

(a) (b)

Figure 5.15: PLF value for the right arm for one contraction divided in 5 windows of 500 points (obtaining 5 values of PLF). The blue vertical line indicates the maximum value of PLF. (a) Results for 17 Hz for the member of the patient group (PLF is 0.955 for the window 4). (b) Results for 17 Hz for the member of the control group (PLF is 0.662 for the window 0).

5.3 FD analysis

5.3.1 FD Results

Figure 5.16 presents an average of the linear relationship of base 10 logarithm of $L(k)$ for each value of k estimated among all subjects within each group.

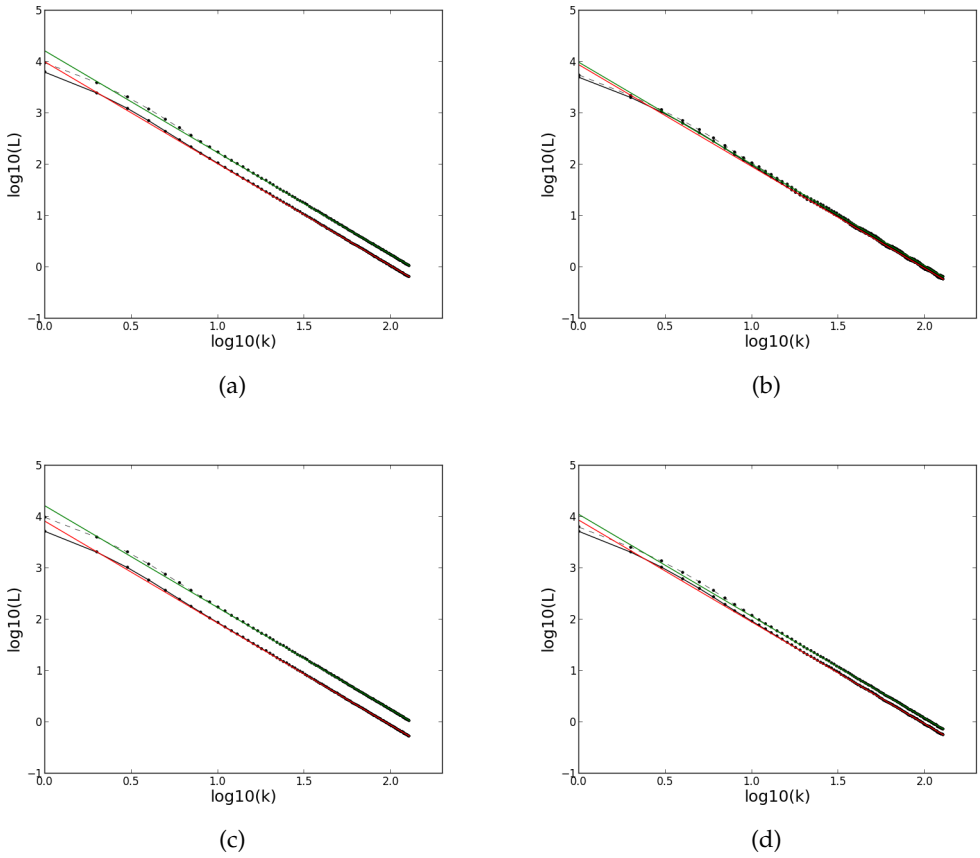

Figure 5.16: Average of the base 10 logarithm of $L(k)$ plotted against k for both groups. The red straight lines correspond to the linear regressions for the patients group. The green straight lines correspond to the linear regressions for the control group. (a) Left hand; the curve fitting is described by $-1.98x+4.00$ for the patient group and by $-1.98x+4.21$ for the control group (b) Left forearm; the curve fitting is described by $-1.98x+3.94$ for the patient group and by $-1.98x+3.99$ for the control group (c) Right hand; the curve fitting is described by $-1.99x+3.91$ for the patient group and by $-1.98x+4.21$ for the control group (d) Right forearm; the curve fitting is described by $-1.98x+3.93$ for the patient group and by $-1.98x+4.04$ for the control group.

FD coefficient mean and standard deviation values are presented in Table 5.2, for the group of patients and the group of control.

From the observation of Table 5.2 FD coefficient is almost identical for both groups. Therefore, FD coefficient is not a good measure of distinction between patients and control group. However, the obtained FD values are very similar to the results obtained from

different upper limb activities in [25]. Observing the graphics shown in Figure 5.16, $L(k)$ is generally superior for the control group than for the patients group. In fact, the point of lowest scale, which is the point of intersection on the y-axis, is the MFL. Observing Figure 5.16, MFL is always slightly higher for the control group. Table 5.3 represents the MFL values for each group, presenting slightly higher MFL values for the control group.

Table 5.2: Mean and standard deviation values of FD coefficient for patients and control group.

	Patients group	**Control group**
Left hand	-1.984 ± 0.011	-1.983 ± 0.007
Left forearm	-1.982 ± 0.008	-1.983 ± 0.006
Right hand	-1.985 ± 0.008	-1.983 ± 0.008
Right forearm	-1.983 ± 0.013	-1.984 ± 0.006

Table 5.3: MFL values for patients and control group.

	Patients group	Control group
Left hand	3.80 ± 0.29	3.98 ± 0.20
Left forearm	3.70 ± 0.42	3.74 ± 0.27
Right hand	3.72 ± 0.39	3.99 ± 0.20
Right forearm	3.72 ± 0.47	3.80 ± 0.22

5.4 LZ analysis

5.4.1 LZ Results

For each signal, the LZ coefficient was calculated for instants of contraction with three different binary sequences. Table 5.4 shows the LZ coefficient mean value and standard deviation for a binary sequence obtained for the filtered used signal with threshold defined as 0, Table 5.5 for a binary sequence obtained from the rectified filtered used signal with threshold defined as 0.4 and Table 5.6 for a binary sequence obtained from the envelope of the rectified filtered used signal with threshold defined as 0.12.

From the observation of Table 5.4, LZ coefficient presents very similar values for both patient and control groups. However, this coefficient presents slightly higher values for the patients group for both left and right hands, and slightly higher values for the control group for both left and right forearms.

From the observation of Table 5.5, LZ coefficient presents more distinct values. However, in contradiction with Table 5.4, this coefficient presents smaller values for the patients group for both left and right hands, and smaller values for the control group for both left and right forearms.

The results presented in Table 5.6 are very similar among both groups, however, more

in conformity with those presented in Table 5.5, with slightly smaller values for the patients group for both left and right hands. The differences in these results are explained by the used binary sequence. Table 5.6 presents smaller values since the envelope of the rectified filtered signal is used, which originates fewer different patterns and, hence, a smaller LZ coefficient.

Comparing the results from Tables 5.4, 5.5 and 5.6, it is possible to say that the used binary sequence may influence the LZ tendency according to the acquired signal.

Tables 5.4 and 5.5 present a better distinction between patient and control groups, Table 5.5 with a higher standard deviation and Table 5.4 with a smaller standard deviation. Therefore, for a binary sequence obtained from the filtered used signal and for a binary sequence obtained from the rectified filtered used signal, LZ pooled coefficient values evidence some differences between subjects from both groups, however, with some variance among subjects within each group.

Table 5.4: LZ coefficient for a binary sequence obtained from the filtered used signal with threshold defined as 0.

	Patients group	**Control group**
Left hand	1.25 ± 0.07	1.23 ± 0.06
Left forearm	1.19 ± 0.08	1.22 ± 0.07
Right hand	1.25 ± 0.05	1.23 ± 0.04
Right forearm	1.20 ± 0.06	1.22 ± 0.05

Table 5.5: LZ coefficient for a binary sequence obtained from the rectified filtered used signal with threshold defined as 0.4.

	Patients group	**Control group**
Left hand	0.22 ± 0.17	0.28 ± 0.19
Left forearm	0.24 ± 0.20	0.16 ± 0.12
Right hand	0.17 ± 0.13	0.27 ± 0.16
Right forearm	0.27 ± 0.29	0.15 ± 0.13

Table 5.6: LZ coefficient for a binary sequence obtained from the envelope of the rectified filtered used signal with threshold defined as 0.12.

	Patients group	**Control group**
Left hand	0.100 ± 0.017	$0,113 \pm 0.015$
Left forearm	0.104 ± 0.021	0.098 ± 0.018
Right hand	0.092 ± 0.012	0.115 ± 0.018
Right forearm	0.098 ± 0.015	0.099 ± 0.017

5.5 DFA analysis

5.5.1 DFA Tests

As referred in section 2.2.3.5, DFA's scaling exponent is expected to assume specific values according to the time series behavior. The base 10 logarithm of $F(n)$ was plotted against n (Figure 5.17) for White, Pink and Brownian noise.

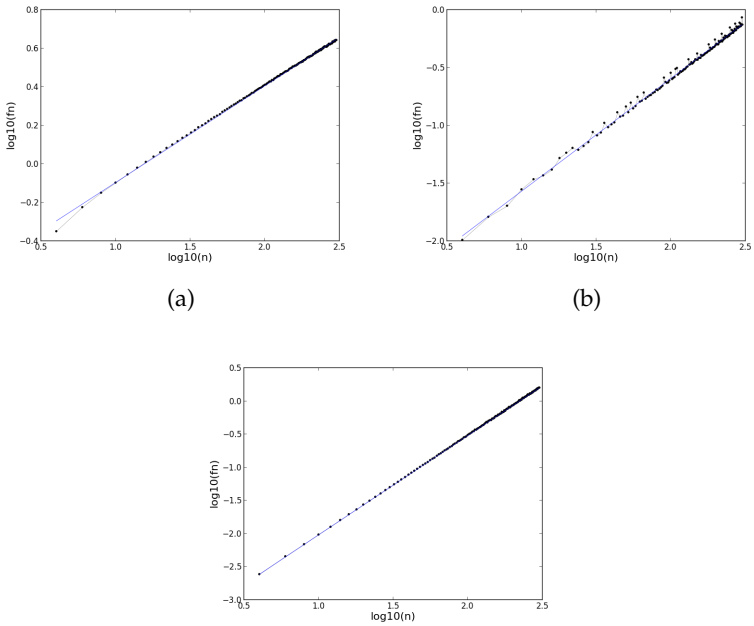

(a) (b)

(c)

Figure 5.17: Base 10 logarithm of $F(n)$ plotted against n for (a) White noise for a signal with 300000 ms ($\alpha = 0,502$); (b) Pink noise for a signal with 297000 ms ($\alpha = 0,974$); (c) Brownian noise for a signal with 300000 ($\alpha = 1,499$).

DFA's scaling exponent, α, assumes the value $\alpha = 0,502$ for White noise, $\alpha = 0,974$ for Pink noise and $\alpha = 1,499$ for Brownian noise, which is consistent with the expected values referred in section 2.2.3.5.

5.5.2 DFA Results

Figure 5.18 represents the linear relationship of base 10 logarithm of $F(n)$ for each value of n averaged among all subjects within each group.

Tables 5.7 and 5.8 present the DFA coefficients, α_1 and α_2 mean values for both groups, respectively.

As observed in Figure 5.18, the linear relationship of base 10 logarithm of $F(n)$ for each value of n presents higher values for the control group for both left and right hands, and higher values for the patients group for both left and right forearms.

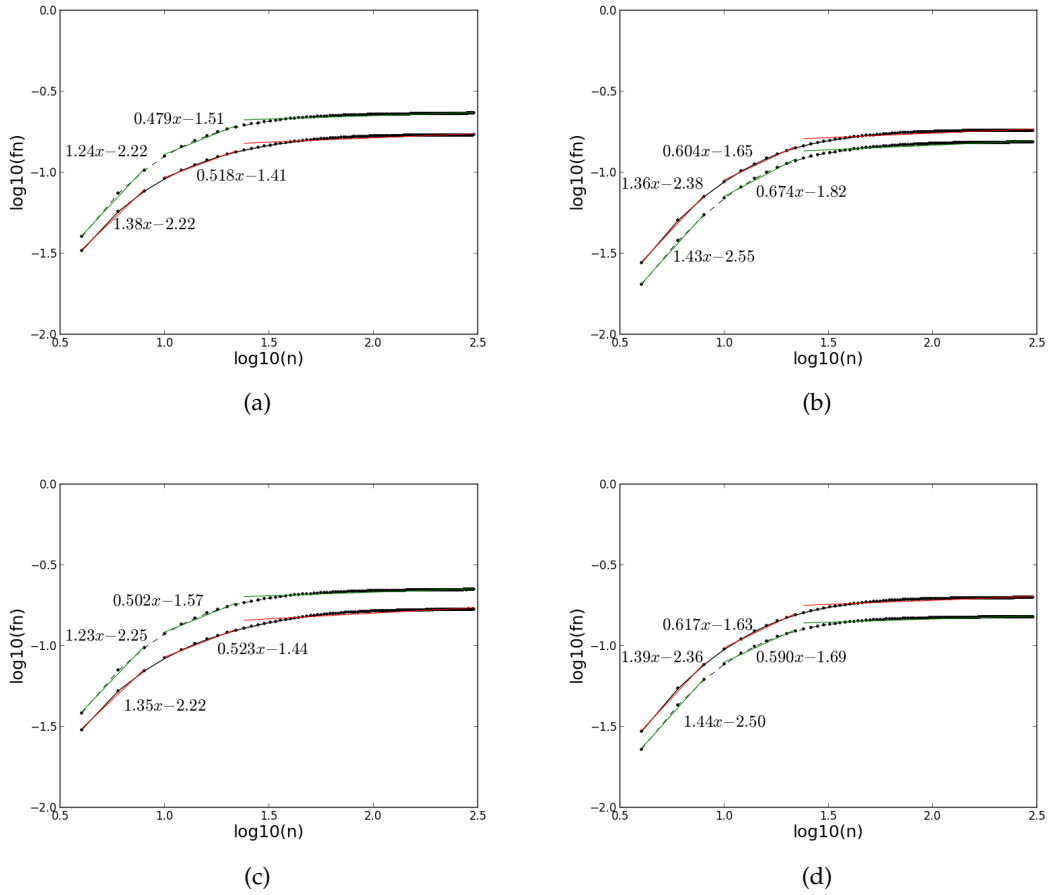

Figure 5.18: Base 10 logarithm of $F(n)$ plotted against n averaged among all subjects within each group. The black dashed line corresponds to the patient group and the black straight line corresponds to the control group. The red straight lines correspond to the linear regressions of each segment for the patients group. The green straight lines correspond to the linear regressions of each segment for the control group. The curve fitting for each segment is shown in the graph. (a) Results for the left hand. (b) Results for the left forearm. (c) Results for the right hand. (d) Results for the right forearm.

Table 5.7: DFA α_1 coefficient mean and standard deviation values for both groups.

	Patients group	Control group
Left hand	1.24 ± 0.20	1.38 ± 0.16
Left forearm	1.36 ± 0.28	1.43 ± 0.15
Right hand	1.23 ± 0.17	1.35 ± 0.14
Right forearm	1.39 ± 0.09	1.44 ± 0.11

Table 5.8: DFA α_2 coefficient mean and standard deviation values for both groups.

	Patients group	Control group
Left hand	$0,48 \pm 0.11$	$0,52 \pm 0.10$
Left forearm	0.60 ± 0.14	0.67 ± 0.13
Right hand	0.50 ± 0.12	0.52 ± 0.09
Right forearm	0.62 ± 0.16	0.59 ± 0.10

As observed in Tables 5.7 and 5.8, DFA coefficients present higher values for the control group. Therefore, DFA algorithm appears to distinguish both groups.

5.6 MSE analysis

5.6.1 MSE Tests

Figure 5.19 shows the Sample Entropy value for each scale concerning White and Pink noise for a signal with length 80 s with used tolerance $r = 0.15\sigma$.

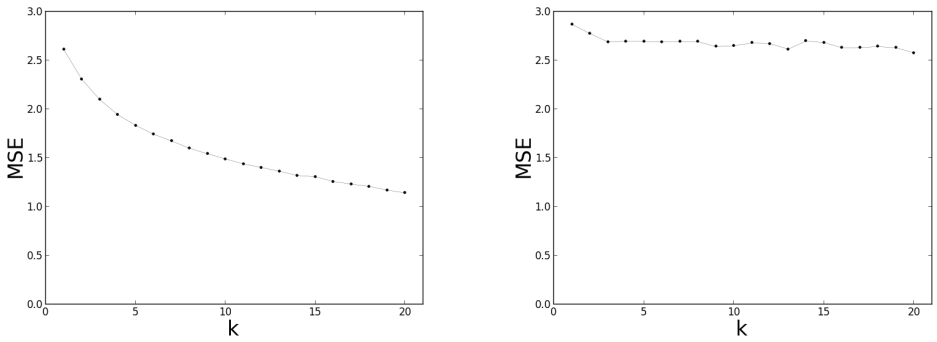

(a) (b)

Figure 5.19: Schematic representation of the Sample Entropy value for each scale (each τ) for a signal with length 80 s. The used tolerance is $r = 0.15\sigma$. (a) Results for White noise. (b) Results for Pink noise.

Figure 5.19 shows a decreasing in entropy with the scale factor for White noise and a constant value of entropy with the scale factor for Pink noise, as it was expected [47]. White and Pink noise were also tested for a tolerance $r = 0.15$, with similar results, as well as for longer signals.

5.6.2 MSE Results

Figure 5.20 represents the Sample Entropy mean value for each scale for both patient and control groups for tolerance, τ, of 0.15σ.

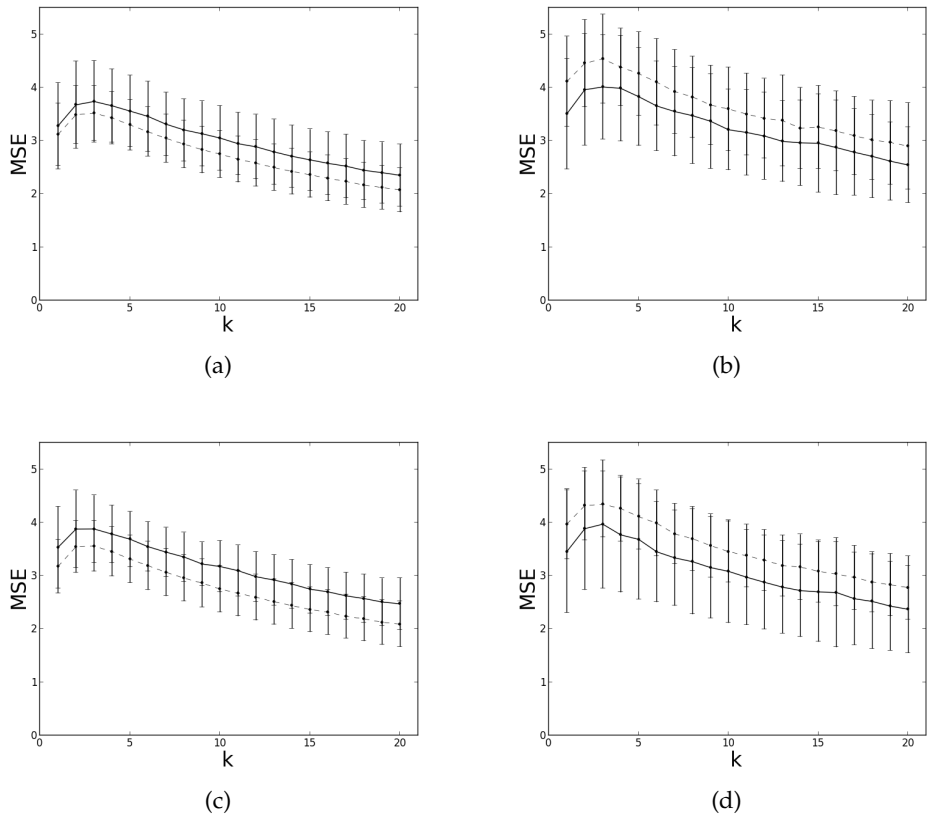

Figure 5.20: Sample Entropy mean value for each scale obtained for tolerance, τ, of 0.15σ. The straight line represents the patient group, and the dashed line represents the control group. (a) Results for the left hand. (b) Results for the left forearm. (c) Results for the right hand. (d) Results for the right forearm.

MSE pooled values for the patients and control groups are presented in table 5.9.

Table 5.9: MSE mean and standard deviation values, for both patients and control groups.

	Patients group	**Control group**
Left hand	3.01 ± 0.45	2.75 ± 0.47
Left forearm	3.26 ± 0.46	3.64 ± 0.52
Right hand	3.15 ± 0.46	2.77 ± 0.48
Right forearm	3.08 ± 0.49	3.50 ± 0.52

Observing Figure 5.20, patients group exhibit higher entropies for both left and right hands, whereas control group exhibit higher entropies for both left and right forearms. The MSE tendency exhibited in Figure 5.20 occurs since the sampling time is smaller than the correlation time in the sampled data, as discussed previously.

Observing the results presented in Figure 5.20 and Table 5.9, MSE algorithm appears to be capable of distinguish both groups, however with some variance within each group.

5.7 One Long Contraction

In order to compare the results reached with one single contraction with those obtained by averaging several contractions, one long contraction, with 179150 ms, was studied regarding all algorithms. This analysis was only executed for a healthy subject. An example of the acquired signals is represented in figure 5.21.

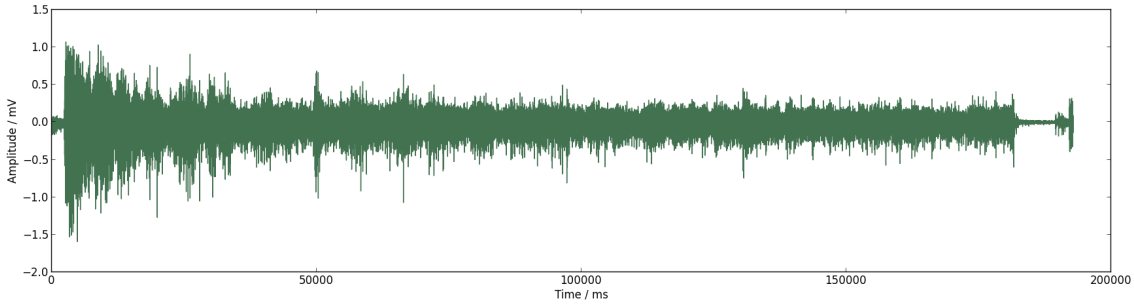

Figure 5.21: Signal from the right hand acquired from a healthy subject (moment of contraction with 179150 ms).

Figure 5.22 shows coherence results for both arms.

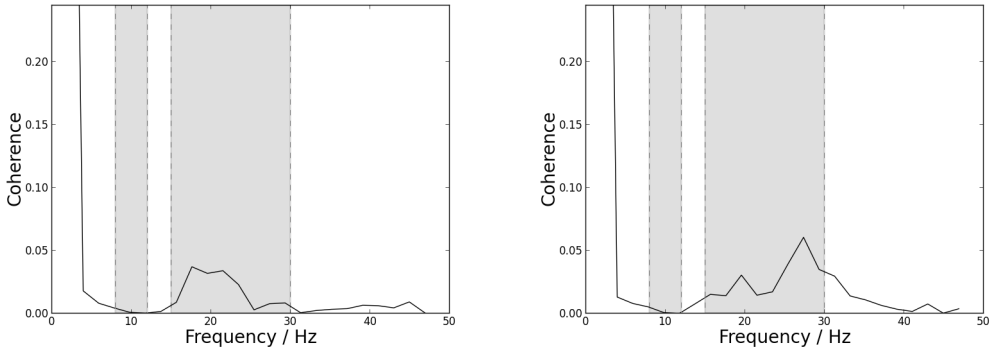

(a) (b)

Figure 5.22: Coherence values dependency on frequency for one long contraction of a healthy subject with NFFT placed as 512. Straight line for patients and dashed line for controls. The first grey box delimitates the frequencies corresponding to the alpha band ($8 - 12$ Hz). The second grey box delimitates the frequencies corresponding to the beta band ($15 - 30$ Hz). (a) Results from the left arm. (b) Results from the right arm.

Coherence values observed in Figure 5.22, are much lower than the coherence mean values for the control group obtained for an averaging of several smaller contractions. However, for this particular control, coherence values regarding beta band frequencies

seem enhanced when compared to those obtained for most members of the control group. Coherence mean value is 0.01 ± 0.02 for the left arm and 0.01 ± 0.02 for the right arm.

Figure 5.23 shows PLF results for both arms.

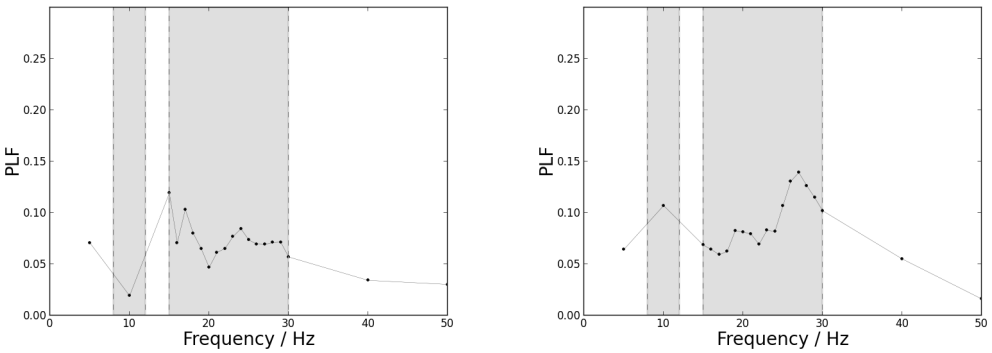

(a) (b)

Figure 5.23: PLF values dependency on frequency for one long contraction of a healthy subject. The first grey box delimitates the frequencies corresponding to the alpha band ($8 - 12$ Hz). The second grey box delimitates the frequencies corresponding to the beta band ($15 - 30$ Hz).(a) Results from the left arm. (b) Results from the right arm.

Observing Figure 5.23, it is possible to verify that PLF values decrease when calculated for longer instants of contraction, which confirms higher PLF values for shorter instants, as it was said previously. For this particular subject, beta band frequencies seem enhanced comparatively to the others. Alpha band seems enhanced only for the right arm for this particular subject. PLF mean value is 0.06 ± 0.03 for the left arm and $0,08 \pm 0,03$ for the right arm.

The FD coefficient is: $-1,99$ for the left hand; $-1,98$ for the left forearm; $-1,99$ for the right hand; and $-1,99$ for the right forearm. MFL is 4.02 for the left hand; 3.83 for the left forearm; 4.10 for the right hand; and 3.86 for the right forearm. These results are very similar to those obtained for the control group for the concatenation of all the contractions.

The LZ coefficient for a binary sequence obtained from the filtered used signal is: $1,27$ for the left hand; $1,18$ for the left forearm; $1,26$ for the right hand; and $1,23$ for the right forearm. These results do not appear to be significantly different from those obtained for the control group for the concatenation of all the contractions.

Table 5.10 contains the DFA coefficients values, α_1 and α_2 for one control for one long contraction. The presented results are very similar to those obtained for the control group for the concatenation of all the contractions.

Figure 5.24 shows the Sample Entropy value for each scale for one long contraction of a healthy subject for tolerance, τ, of 0.15σ.

MSE mean and standard deviation values for one contraction of a healthy subject are: $2,79 \pm 0,57$ for the left hand; $3,28 \pm 0,53$ for the left forearm; $2,59 \pm 0,56$ for the right

Table 5.10: DFA coefficients values, α_1 and α_2, for one control for one long contraction of a healthy subject with 179150 ms.

	$\alpha 1$	$\alpha 2$
Left hand	1.32	$0,52$
Left forearm	1.50	0.64
Right hand	1.35	0.50
Right forearm	1.44	0.58

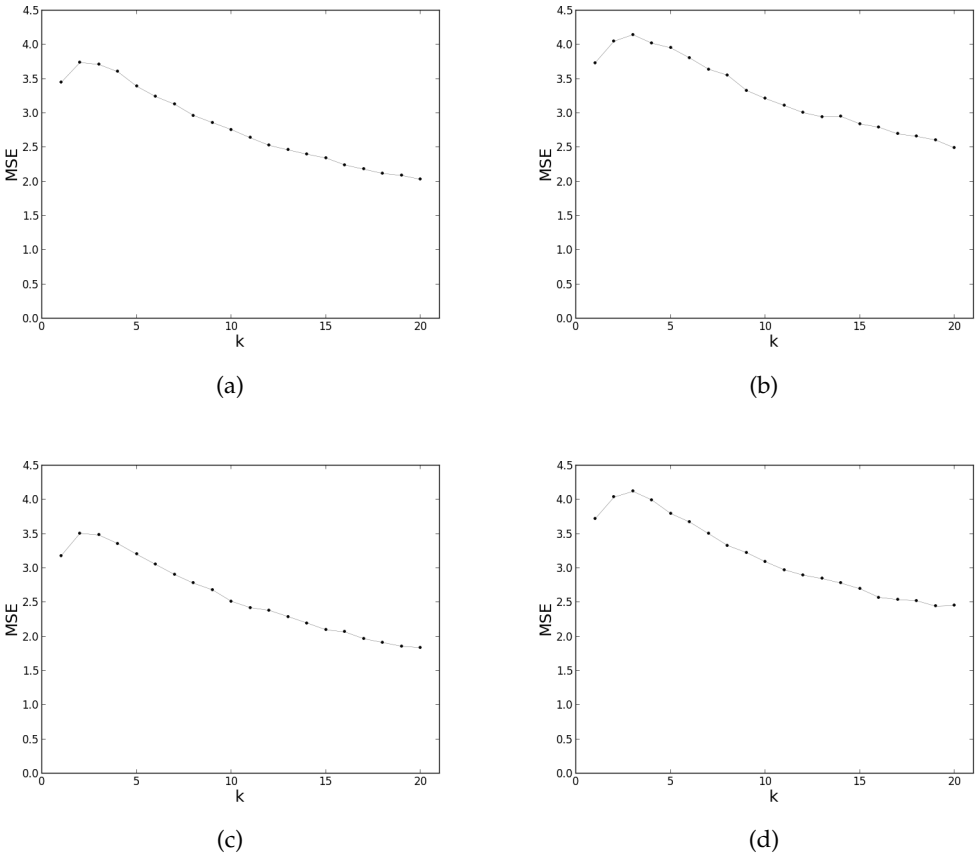

Figure 5.24: Sample Entropy value for each scale for one long contraction of a healthy subject for tolerance, τ, of 0.15σ. (a) Results for the left hand. (b) Results for the left forearm. (c) Results for the right hand. (d) Results for the right forearm.

hand; and $3,16 \pm 0,56$ for the right forearm.

Results seem to be similar to those obtained for the mean Sample Entropy values for the control group, since entropy values are slightly higher for both left and right forearms than for left and right hands.

To conclude, one long contraction appears to enhance both coherence and PLF within the beta band frequencies, however with decrease in their values comparing to an average of several smaller contractions. Regarding FD, LZ, DFA and MSE algorithms, results for one long contraction seem to be very similar to those obtained for the application of

these algorithms for the concatenation of all contractions. It is important to remember that this analysis was executed only for one healthy subject, and only a larger statistic group would provide more confident results.

5.8 Classification Results

As previously described in section 4.4, several combinations of parameters were tested. Table 5.11 presents the 14 combinations and the 3 classifiers with better results for the right arm for a Leave-one-out cross validation.

Table 5.11: Classification results for the right arm for Decision Tree, Random Forest and AdaBoost Classifiers.

Combinations	Decision Tree	Random Forest	AdaBoost
Right Hand			
sum power band + MSE + DFA (α_1 + α_2)	0,806	0,694	0,722
mean + MSE + DFA (α_1 + α_2)	0,806	0,778	0,722
mean + MSE + DFA (α_1 + α_2) + LZ	0,833	0,611	0,750
spectral skewness + MSE + DFA α_1 + α_2) + LZ	0,806	0,667	0,667
spectral spread + MSE + DFA (α_1 + α_2) + LZ	0,806	0,639	0,722
Right Forearm			
spectral kurtosis + MSE + DFA (α_1 + α_2) + LZ	0,667	0,750	0,806
Right Arm			
sum power band + MSE + coherence + PLF + DFA (α_1 + α_2)	0,778	0,750	0,806
kurtosis + MSE + DFA (α_1 + α_2)	0,556	0,750	0,806
kurtosis + MSE + DFA (α_1 + α_2) + LZ	0,500	0,806	0,778
kurtosis + MSE + coherence + PLF + DFA (α_1 + α_2)	0,694	0,833	0,694
maximum frequency + MSE + coherence + PLF + DFA (α_1 + α_2)	0,667	0,611	0,806
mean +MSE + DFA (α_1 + α_2)	0,556	0,806	0,639
spectral skewness + MSE + coherence + DFA (α_1 + α_2)	0,667	0,861	0,750
spectral spread +MSE + coherence + PLF + DFA (α_1 + α_2)	0,694	0,833	0,694

Tables B.1, B.2 and B.3 of Appendix B present the classification results for the right arm for a Leave-one-out cross validation tested with k - Nearest Neighbor, Decision Tree, Random Forest, AdaBoost and Naïve Bayes classifiers. In spite of 201 combinations have been arranged, only the best results are shown.

Classification results demonstrate the algorithms distinction capability, since the presented results show the percentage of cases that the algorithm classified correctly (accuracy percentage).

Classification results were obtained for the right arm for a leave-one-out cross validation tested with k - Nearest Neighbor, Decision Tree, Random Forest, AdaBoost and Naïve Bayes classifiers. In spite of 201 combinations have been arranged, 118 combinations present values higher than 70.0% for at least one classifier, 41 combinations present results higher than 77.8% for at least one classifier, and 14 combinations present results higher than 80.6% for one classifier (Decision Tree, Random Forest or AdaBoost).

For the right arm, the best results include MSE, DFA, LZ, coherence and PLF algorithm results, and also the extracted features mean, maximum frequency, spectral kurtosis, spectral skewness, spectral spread, sum power band and kurtosis, in several different combinations. The top 14 best combinations include the results of both DFA and MSE algorithms. The best obtained combination is spectral skewness + MSE + coherence + DFA (α_1 and α_2), with an accuracy percentage of 86.1% for a Random Forest Classifier. Therefore, it is proved that in spite of some algorithms may present slender differences between both control and patients group, the combination of these algorithms with other measures can improve the distinction capability between members of patients and control groups.

6

Conclusions

During this work, a set of algorithms were developed to analyze the dynamic of the sEMG signals acquired from different muscle groups of healthy subjects and patients with ALS. FD, LZ, DFA and MSE algorithms were implemented and all of these algorithms as well as coherence and PLF algorithms were applied to the acquired filtered signals. Coherence and PLF algorithms were both tested and validated with synthetic signals. Coherence tests proved that this algorithm behaves as supposed, which guarantees its correct application. Coherence between a signal and itself result in a coherence value of 1, and coherence between two random signals assumes values very close to 0. Synthetic cosine signals, with a random phase component and with a specific known frequency were used to test PLF algorithm. PLF assumes values very close to 1 for the double of the used signal frequency, since this algorithm is applied to the full-wave rectified signal.

White, Pink and Brownian noise signals were generated to test some of the algorithms: the first two were used to test MSE algorithm, and DFA algorithm was tested for the all three, being the results consistent with those presented in literature [47, 25].

All algorithms were also tested for a long contraction, being the results very similar to those obtained for the concatenation of all the contractions for FD, LZ, DFA and MSE algorithms. Both coherence and PLF algorithms assume lower values concerning a long contraction, being the values obtained with those algorithms enhanced for the beta band frequencies.

Contrary to the results presented in literature, both coherence and PLF analysis in ipsilateral acquisitions do not present significant differences between the group of patients and the group of control. Results from both algorithms appear to be slightly higher for the control group for the alpha band frequencies. For further work is suggested to

compute PLF for all the frequencies within the alpha band with resolution of 1 Hz.

Coherence appears to present the same tendency for the same signal with different lengths (the same peaks of coherence are observed for the same frequency). However, for one signal divided in several parts with the same length, coherence peaks appear to be more dispersed within a range of frequencies.

Coherence also appears to present the same behavior for both contraction and relaxation moments when computed and plotted for each contraction/relaxation, presenting very distinct values according to the contraction/relaxation number.

Maximum coherence does not appear to be associated to a specific frequency, since all subjects among both groups present maximum coherence for different frequencies.

Regarding PLF, it was not possible to obtain a consistent time lag associated to the maximum PLF value within one contraction.

FD analysis results in FD coefficients very similar for all the four signals for both patients and control groups. Therefore, this algorithm does not seem good to obtain a distinction between both groups. However, MFL presents slightly higher values regarding the control group, being this a better measure of distinction between both groups than the FD coefficient.

LZ analysis presents better results, being LZ coefficient higher for the control group for both left and right hands, and higher for the patients group for both left and right forearms. These results are for a binary sequence obtained from the rectified filtered used signal. Therefore, LZ coefficient appears to be a good reflection of the presence of ALS. Since the used threshold to obtain the binary sequence was defined as 0.4, it is not adapted to each individual signal. Therefore, it is suggested for further work a threshold obtained as a percentage of the standard deviation of each signal.

DFA analysis presents higher values for both α_1 and α_2 coefficients for the control group. Then, this algorithm seems to be a good measure to reflect the presence of ALS.

Setting the tolerance τ as 0.15σ, MSE analysis presents higher values for both left and right hands for the patients group, and higher values for both left and right forearms for the control group. This algorithm appears to be a good indicator of the presence of ALS.

Both LZ and MSE results exhibit different tendencies regarding hands and forearms for both patient and control's groups. Both LZ (concerning a binary sequence obtained for the filtered used signal with threshold defined as 0) and MSE results show higher values for both hands for the group of patients, and higher values for both forearms for the control group. This tendency appears to also occur for the FD results, however not in a very significant manner. However, when the binary sequence is obtained from the rectified filtered used signal with threshold defined as 0.4, the tendency observed for the LZ results is inverted.

LZ, DFA and MSE analysis have then potential as a quantitative test for upper and lower neural integrity concerning ALS disease.

Classification results demonstrate to provide a good distinction of both groups, being the combination of various algorithms with features proved to be advantageous to

improve the distinction capability between both groups.

The algorithms analysis was performed for both left and right arms for the majority of the members of the patients group. Each patient presents a different disease stage, as well as a different onset form, reason why each patient presents different motor limitation levels for each arm. A better statistical estimation would be obtained for groups of patients assembled according to the onset form or the diagnostic time. This analysis has been executed for coherence only, and significant differences are obtained within the patients group. Therefore, a higher number of patients presenting each onset form would be preferable for better statistical results. In further work, it is suggested to execute this analysis regarding different onset forms for the other algorithms, since in spite of mean results present differences between both groups, individual results for each subject present a certain variance within each group.

Members from both groups suggested some alterations to the acquisition protocol: longer times of contraction and longer times of relaxation. This alteration to the protocol is then proposed, for example 6 seconds of contraction and 6 seconds of relaxation, in order to facilitate the task performance. This alteration would not compromise the results regarding FD, LZ, DFA and MSE algorithms, since they were tested for one long contraction with the obtainment of similar results. Coherence and PLF algorithms would probably produce different results, since the comparison in results for the average of several small contraction with one long contraction produces different values for both algorithms. However, this alteration may yield better results within the beta band, since these results appear to be enhanced for both algorithms for the analysis of one long contraction.

Since ALS is very difficult to diagnose, and the obtained results exhibit some variance among both groups' subjects, it is important to develop further work in order to find a reliable indicator of this disease's presence/evaluation. The most promissory algorithms are associated to the signal's complexity, and its exploration is then suggested.

Bibliography

[1] Kendra Blatzheim. Interdisciplinary palliative care, including massage, in treatment of amyotrophic lateral sclerosis. *Journal of Bodywork and Movement Therapies*, 13(4):328–335, 2009.

[2] Raafat El-Sayed Shalaby. *Development of an Electromyography Detection System for the Control of Functional Electrical Stimulation in Neurological Rehabilitation*. PhD thesis, Technische Universität Berlin, 2011.

[3] Roberto Merletti, Aleš Holobar, and Dario Farina. Analysis of motor units with high-density surface electromyography. *Journal of electromyography and kinesiology*, 18(6):879–890, 2008.

[4] http://www.quia.com/jg/1369171list.html. Accessed in 17/01/2014.

[5] J Douglas Mitchell and Gian Domenico Borasio. Amyotrophic lateral sclerosis. *The lancet*, 369(9578):2031–2041, 2007.

[6] Orla Hardiman. Amyotrophic lateral sclerosis. In John Wiley & Sons, Ltd, editor, *Encyclopedia of Life Sciences*. John Wiley & Sons, Ltd, Chichester, UK, February 2010.

[7] Anuradha Duleep and Jeremy Shefner. Electrodiagnosis of motor neuron. *Phys Med Rehabil Clin N Am*, 24:139–151, 2013.

[8] Mamede de Carvalho. Why is als so excited? *Clinical Neurophysiology*, 122(9):1689–1690, 2011.

[9] Matthew C Kiernan, Steve Vucic, Benjamin C Cheah, Martin R Turner, Andrew Eisen, Orla Hardiman, James R Burrell, and Margaret C Zoing. Amyotrophic lateral sclerosis. *The Lancet*, 377(9769):942–955, 2011.

[10] Mamede de Carvalho and Michael Swash. The onset of als? *Clinical Neurophysiology*, 121(10):1709–1710, 2010.

[11] Mamede de Carvalho, Reinhard Dengler, Andrew Eisen, John D England, Ryuji Kaji, Jun Kimura, Kerry Mills, Hiroshi Mitsumoto, Hiroyuki Nodera, Jeremy Shefner, et al. Electrodiagnostic criteria for diagnosis of als. *Clinical neurophysiology*, 119(3):497–503, 2008.

[12] Bryan J Traynor, Mary B Codd, Bernadette Corr, Colm Forde, Eithne Frost, and Orla M Hardiman. Clinical features of amyotrophic lateral sclerosis according to the el escorial and airlie house diagnostic criteria: a population-based study. *Archives of neurology*, 57(8):1171, 2000.

[13] Anders Fuglsang-Frederiksen. Diagnostic criteria for amyotrophic lateral sclerosis (als). *Clinical Neurophysiology*, 119(3):495–496, 2008.

[14] Karen M Fisher, Boubker Zaaimi, Timothy L Williams, Stuart N Baker, and Mark R Baker. Beta-band intermuscular coherence: a novel biomarker of upper motor neuron dysfunction in motor neuron disease. *Brain*, 135(9):2849–2864, 2012.

[15] Mamede de Carvalho, Antónia Turkman, and Michael Swash. Motor unit firing in amyotrophic lateral sclerosis and other upper and lower motor neurone disorders. *Clinical Neurophysiology*, 123(11):2312–2318, 2012.

[16] Jacob J Sosnoff, David E Vaillancourt, Lars Larsson, and Karl M Newell. Coherence of emg activity and single motor unit discharge patterns in human rhythmical force production. *Behavioural brain research*, 158(2):301–310, 2005.

[17] P Grosse, MJ Cassidy, and P Brown. Eeg–emg, meg–emg and emg–emg frequency analysis: physiological principles and clinical applications. *Clinical Neurophysiology*, 113(10):1523–1531, 2002.

[18] Claire L Witham, C Nicholas Riddle, Mark R Baker, and Stuart N Baker. Contributions of descending and ascending pathways to corticomuscular coherence in humans. *The Journal of physiology*, 589(15):3789–3800, 2011.

[19] Simon F Farmer, John Gibbs, David M Halliday, Linda M Harrison, Leon M James, Margaret J Mayston, and John A Stephens. Changes in emg coherence between long and short thumb abductor muscles during human development. *The Journal of physiology*, 579(2):389–402, 2007.

[20] Sridhar P Arjunan and Dinesh K Kumar. Fractal theory based non-linear analysis of semg. In *Intelligent Sensors, Sensor Networks and Information, 2007. ISSNIP 2007. 3rd International Conference on*, pages 545–548. IEEE, 2007.

[21] Sridhar P Arjunan and Dinesh K Kumar. Fractal properties of surface electromyogram for classification of low-level hand movements from single-channel forearm muscle activity. *Journal of Mechanics in Medicine and Biology*, 11(03):581–590, 2011.

[22] Sridhar Poosapadi Arjunan and Dinesh Kant Kumar. Computation of fractal features based on the fractal analysis of surface electromyogram to estimate force of contraction of different muscles. *Computer Methods in Biomechanics and Biomedical Engineering*, 17(3):210–216, 2014.

[23] Mehran Talebinejad, Adrian DC Chan, and Ali Miri. A lempel–ziv complexity measure for muscle fatigue estimation. *Journal of Electromyography and Kinesiology*, 21(2):236–241, 2011.

[24] Leonardo Sarlabous, Abel Torres, José A Fiz, Josep Morera, and Raimon Jané. Index for estimation of muscle force from mechanomyography based on the lempel–ziv algorithm. *Journal of Electromyography and Kinesiology*, 2013.

[25] Angkoon Phinyomark, Pornchai Phukpattaranont, Chusak Limsakul, and Montri Phothisonothai. Electromyography (emg) signal classification based on detrended fluctuation analysis. *Fluctuation and Noise Letters*, 10(03):281–301, 2011.

[26] Prodromos A Kaplanis, Constantinos S Pattichis, Damjan Zazula, et al. Multiscale entropy-based approach to automated surface emg classification of neuromuscular disorders. *Medical & biological engineering & computing*, 48(8):773–781, 2010.

[27] Xu Zhang, Xiang Chen, Paul E Barkhaus, and Ping Zhou. Multiscale entropy analysis of different spontaneous motor unit discharge patterns. *Journal of Biomedical and Health Informatics*, 17(2), 2013.

[28] Ranjit A Thuraisingham and Georg A Gottwald. On multiscale entropy analysis for physiological data. *Physica A: Statistical Mechanics and its Applications*, 366:323–332, 2006.

[29] Bjoern M Eskofier, Martin Kraus, Jay T Worobets, Darren J Stefanyshyn, and Benno M Nigg. Pattern classification of kinematic and kinetic running data to distinguish gender, shod/barefoot and injury groups with feature ranking. *Computer methods in biomechanics and biomedical engineering*, 15(5):467–474, 2012.

[30] Kang Soo Kim, Heung Ho Choi, Chang Soo Moon, and Chi Woong Mun. Comparison of< i> k</i>-nearest neighbor, quadratic discriminant and linear discriminant analysis in classification of electromyogram signals based on the wrist-motion directions. *Current Applied Physics*, 11(3):740–745, 2011.

[31] Li-Min Wang, Xiao-Lin Li, Chun-Hong Cao, and Sen-Miao Yuan. Combining decision tree and naive bayes for classification. *Knowledge-Based Systems*, 19(7):511–515, 2006.

[32] Xu Zhang, Xiang Chen, Yun Li, Vuokko Lantz, Kongqiao Wang, and Jihai Yang. A framework for hand gesture recognition based on accelerometer and emg sensors. *Systems, Man and Cybernetics, Part A: Systems and Humans, IEEE Transactions on*, 41(6):1064–1076, 2011.

[33] Marie-Hélène Roy and Denis Larocque. Robustness of random forests for regression. *Journal of Nonparametric Statistics*, 24(4):993–1006, 2012.

[34] Dan Stashuk. Emg signal decomposition: how can it be accomplished and used? *Journal of Electromyography and Kinesiology*, 11(3):151–173, 2001.

[35] MBI Reaz, MS Hussain, and F Mohd-Yasin. Techniques of emg signal analysis: detection, processing, classification and applications. *Biological procedures online*, 8(1):11–35, 2006.

[36] Geoffrey L Sheean. Quantification of motor unit action potential energy. *Clinical Neurophysiology*, 123(3):621–625, 2012.

[37] Dick F Stegeman, Joleen H Blok, Hermie J Hermens, and Karin Roeleveld. Surface emg models: properties and applications. *Journal of Electromyography and Kinesiology*, 10(5):313–326, 2000.

[38] Roberto Merletti, Alberto Botter, Amedeo Troiano, Enrico Merlo, and Marco Alessandro Minetto. Technology and instrumentation for detection and conditioning of the surface electromyographic signal: state of the art. *Clinical Biomechanics*, 24(2):122–134, 2009.

[39] Pascal Grosse, M Edwards, MAJ Tijssen, A Schrag, Andrew J Lees, KP Bhatia, and Peter Brown. Patterns of emg–emg coherence in limb dystonia. *Movement disorders*, 19(7):758–769, 2004.

[40] Jose M Hurtado, Leonid L Rubchinsky, and Karen A Sigvardt. Statistical method for detection of phase-locking episodes in neural oscillations. *Journal of neurophysiology*, 91(4):1883–1898, 2004.

[41] Miguel Almeida, Ricardo Vigário, and J Bioucas-Dias. Phase locked matrix factorization. In *Proc. of the EUSIPCO Conference*, pages 1728–1732, 2011.

[42] Carlos Carreiras, Luis Borges de Almeida, and J Miguel Sanches. Phase-locking factor in a motor imagery brain-computer interface. In *Engineering in Medicine and Biology Society (EMBC), 2012 Annual International Conference of the IEEE*, pages 2877–2880. IEEE, 2012.

[43] Benoit B Mandelbrot. Stochastic models for the earth's relief, the shape and the fractal dimension of the coastlines, and the number-area rule for islands. *Proceedings of the National Academy of Sciences*, 72(10):3825–3828, 1975.

[44] Hu Xiao, Wang Zhi-zhong, and Ren Xiao-mei. Classification of surface emg signal with fractal dimension. *Journal of Zhejiang University Science B*, 6(8):844–848, 2005.

[45] Jingdong Zhao, Li Jiang, Hegao Cai, Hong Liu, and Gerd Hirzinger. A novel emg motion pattern classifier based on wavelet transform and nonlinearity analysis method. In *Robotics and Biomimetics, 2006. ROBIO'06. IEEE International Conference on*, pages 1494–1499. IEEE, 2006.

[46] RB Govindan, JD Wilson, H Eswaran, CL Lowery, and H Preißl. Revisiting sample entropy analysis. *Physica A: Statistical Mechanics and its Applications*, 376:158–164, 2007.

[47] Madalena Costa, C-K Peng, Ary L Goldberger, and Jeffrey M Hausdorff. Multiscale entropy analysis of human gait dynamics. *Physica A: Statistical Mechanics and its applications*, 330(1):53–60, 2003.

[48] F. Pedregosa, G. Varoquaux, A. Gramfort, V. Michel, B. Thirion, O. Grisel, M. Blondel, P. Prettenhofer, R. Weiss, V. Dubourg, J. Vanderplas, A. Passos, D. Cournapeau, M. Brucher, M. Perrot, and E. Duchesnay. Scikit-learn: Machine learning in Python. *Journal of Machine Learning Research*, 12:2825–2830, 2011.

[49] Fabien Lotte, Marco Congedo, Anatole Lécuyer, Fabrice Lamarche, Bruno Arnaldi, et al. A review of classification algorithms for eeg-based brain–computer interfaces. *Journal of neural engineering*, 4, 2007.

[50] Jung Hwan Cho and Pradeep U Kurup. Decision tree approach for classification and dimensionality reduction of electronic nose data. *Sensors and Actuators B: Chemical*, 160(1):542–548, 2011.

[51] Mafalda Camara. Coherence and phase locking disruption in electromyograms of patients with amyotrophic lateral sclerosis. Master's thesis, Faculdade de Ciências e Tecnologia da Univerisade Nova de Lisboa, 2013.

[52] Guan Wenye. http://www.mathworks.com/matlabcentral/fileexchange/19795-detrended-fluctuation-analysis/content/dfa/dfa_main.m, 2009. Accessed in 04/03/2014.

[53] Yu-Hsiang Pan, Wei-Yen Lin, Yung-Hung Wang, and Kuo-Tien Lee. Computing multiscale entropy with orthogonal range search. *Journal of Marine Science and Technology*, 19(1):107–113, 2011.

[54] http://www.psynetresearch.org/uploads/7/5/8/1/7581337/msentropy.rar. Accessed in 23/05/2014.

[55] http://wiki.scipy.org/cookbook/brownianmotion. Accessed in 21/03/2014.

[56] Ana Luísa Gomes. Human activity recognition with accelerometry: Novel time and frequency features. Master's thesis, Faculdade de Ciências e Tecnologia da Universidade Nova de Lisboa, 2014.

Appendix A

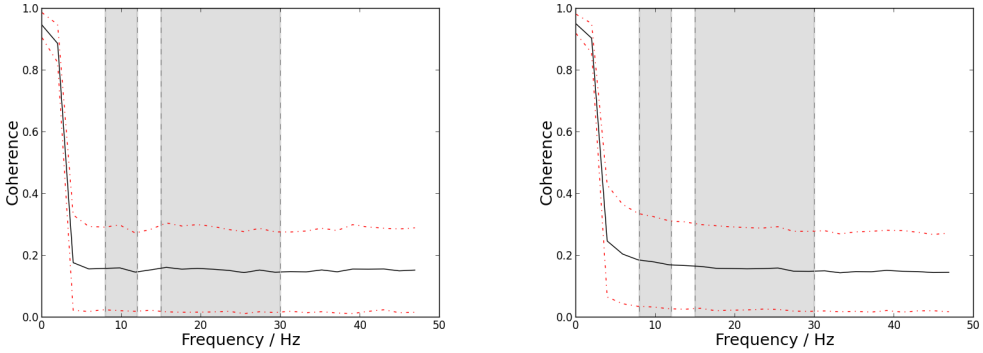

(a) (b)

Figure A.1: Mean coherence values dependency on frequency (straight line) and standard deviation (dotted red line) for the patients group. The first grey box delimitates the frequencies corresponding to the alpha band ($8-12$ Hz). The second grey box delimitates the frequencies corresponding to the beta band ($15-30$ Hz). (a) Results from the left arm. (b) Results from the right arm.

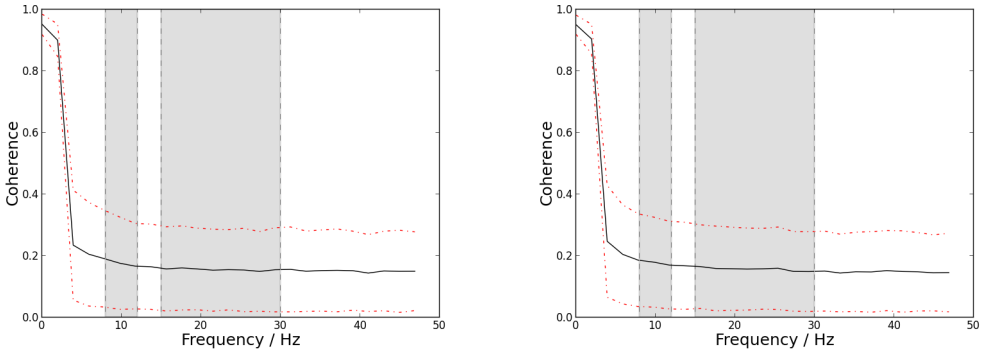

(a) (b)

Figure A.2: Mean coherence values dependency on frequency (straight line) and standard deviation (dotted red line) for the control group. The first grey box delimitates the frequencies corresponding to the alpha band ($8-12$ Hz). The second grey box delimitates the frequencies corresponding to the beta band ($15-30$ Hz). (a) Results from the left arm. (b) Results from the right arm.

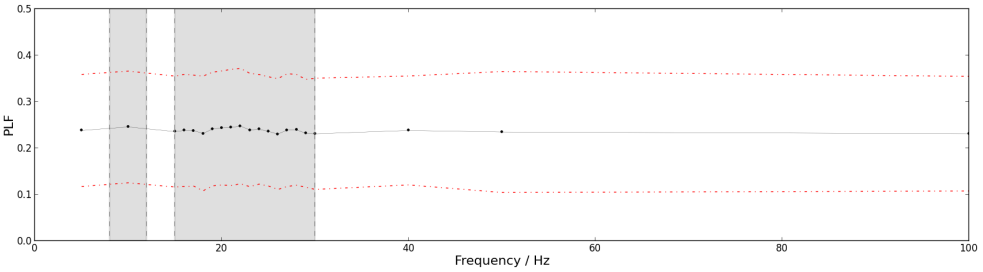

(a)

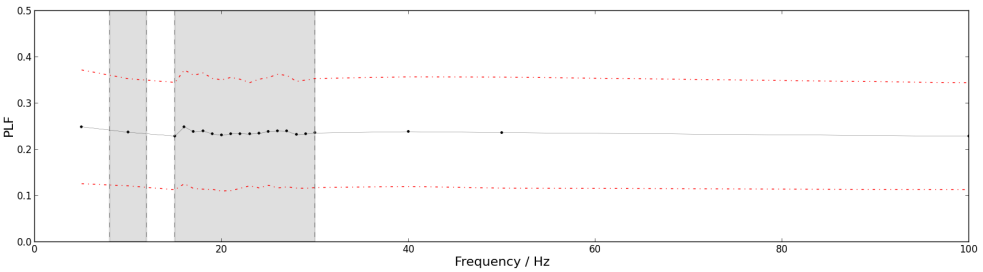

(b)

Figure A.3: Mean PLF values dependency on frequency (straight line) and standard deviation (dotted line) for the patients group. The first grey box delimitates the frequencies corresponding to the alpha band ($8-12$ Hz). The second grey box delimitates the frequencies corresponding to the beta band ($15-30$ Hz). (a) Results from the left arm. (b) Results from the right arm.

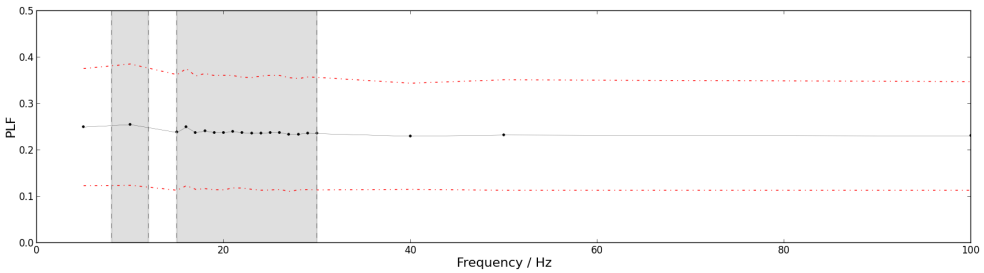

(a)

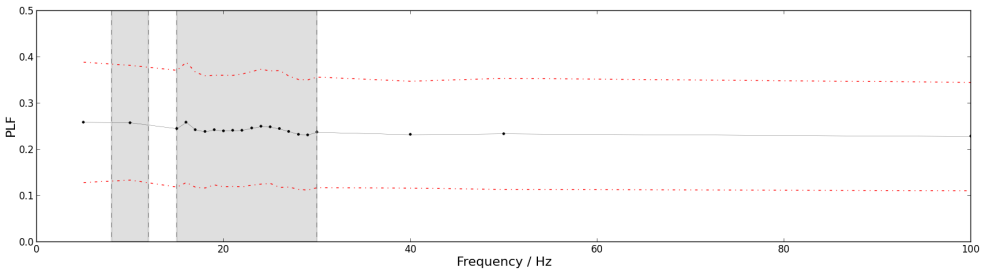

(b)

Figure A.4: Mean PLF values dependency on frequency (straight line) and standard deviation (dotted line) for the control group. The first grey box delimitates the frequencies corresponding to the alpha band ($8 - 12$ Hz). The second grey box delimitates the frequencies corresponding to the beta band ($15 - 30$ Hz). (a) Results from the left arm. (b) Results from the right arm.

Appendix B

Tables B.1, B.2 and B.3 present the classification results for the right arm. Only the best results are shown. From the 201 combinations, 118 combinations present values higher than 0.700 for at least one classifier, and here are presented the best 41 combinations with results higher than 0.778 for at least one classifier. From all the combinations, 14 combinations present results higher than 0.806 for one classifier (Decision Tree, Random Forest or AdaBoost).

Table B.1: Classification results for the right arm for Nearest Neighbors and Decision Tree Classifiers.

Combinations	Nearest Neighbors	Decision Tree
Right Hand		
LZ	0,778	0,750
MSE + FD + LZ + DFA ($\alpha_1 + \alpha_2$)	0,667	0,778
sum power band + MSE + DFA ($\alpha_1 + \alpha_2$)	0,583	0,806
sum power band + MSE + DFA ($\alpha_1 + \alpha_2$) **+ LZ**	0,583	0,778
kurtosis + DFA ($\alpha_1 + \alpha_2$)	0,722	0,778
kurtosis + MSE + DFA ($\alpha_1 + \alpha_2$)	0,694	0,778
kurtosis + MSE + DFA ($\alpha_1 + \alpha_2$) **+ LZ**	0,694	0,778
mean + MSE + DFA ($\alpha_1 + \alpha_2$)	0,667	0,806
mean + MSE + DFA ($\alpha_1 + \alpha_2$) **+ LZ**	0,667	0,833
spectral skewness + MSE + DFA ($\alpha_1 + \alpha_2$) **+ LZ**	0,667	0,806
spectral spread + MSE	0,611	0,778
spectral spread + MSE + DFA ($\alpha_1 + \alpha_2$) **+ LZ**	0,611	0,806
Right Forearm		
spectral spread + MSE + DFA ($\alpha_1 + \alpha_2$) **+ LZ**	0,583	0,694
mean + MSE + DFA ($\alpha_1 + \alpha_2$) **+ LZ**	0,750	0,639
spectral kurtosis + MSE + DFA ($\alpha_1 + \alpha_2$)	0,722	0,667
spectral kurtosis + MSE + DFA ($\alpha_1 + \alpha_2$) **+ LZ**	0,722	0,667
spectral spread + MSE + DFA ($\alpha_1 + \alpha_2$)	0,583	0,639
Right Arm		
MSE + coherence	0,639	0,583
MSE + coherence + DFA ($\alpha_1 + \alpha_2$)	0,639	0,722
sum power band + MSE + coherence + DFA ($\alpha_1 + \alpha_2$)	0,500	0,750
sum power band + MSE + coherence + PLF + DFA ($\alpha_1 + \alpha_2$)	0,500	0,778
kurtosis + DFA ($\alpha_1 + \alpha_2$)	0,722	0,778
kurtosis + MSE + DFA ($\alpha_1 + \alpha_2$)	0,639	0,556
kurtosis + MSE + DFA ($\alpha_1 + \alpha_2$) **+ LZ**	0,639	0,500
kurtosis +MSE + coherence + PLF + DFA ($\alpha_1 + \alpha_2$)	0,639	0,694
max frequency + DFA ($\alpha_1 + \alpha_2$)	0,611	0,611
max frequency + MSE + DFA ($\alpha_1 + \alpha_2$)	0,694	0,583
max frequency + MSE + DFA ($\alpha_1 + \alpha_2$) **+ LZ**	0,694	0,556
max frequency + MSE + coherence + DFA ($\alpha_1 + \alpha_2$)	0,694	0,667
mean + MSE + DFA ($\alpha_1 + \alpha_2$)	0,694	0,556
mean + MSE + DFA ($\alpha_1 + \alpha_2$) **+ LZ**	0,694	0,528
mean + MSE + coherence + PLF + DFA ($\alpha_1 + \alpha_2$)	0,667	0,667
spectral kurtosis + DFA ($\alpha_1 + \alpha_2$)	0,611	0,722
spectral kurtosis + MSE + DFA ($\alpha_1 + \alpha_2$) **+ LZ**	0,667	0,556
spectral kurtosis + MSE + coherence + PLF + DFA ($\alpha_1 + \alpha_2$)	0,667	0,722
spectral skewness + MSE	0,722	0,556
spectral skewness + MSE + coherence + DFA ($\alpha_1 + \alpha_2$)	0,722	0,667
spectral spread + coherence	0,611	0,667
spectral spread + MSE + coherence + DFA ($\alpha_1 + \alpha_2$)	0,611	0,750
spectral spread + MSE + coherence + PLF + DFA ($\alpha_1 + \alpha_2$)	0,611	0,694
All features	0,556	0,750

Table B.2: Classification results for the right arm for Random Forest and AdaBoost Classifiers.

Combinations	**Random Forest**	**AdaBoost**
Right Hand		
LZ	0,694	0,694
MSE + FD + LZ + DFA ($\alpha_1 + \alpha_2$)	0,639	0,694
sum power band + MSE + DFA ($\alpha_1 + \alpha_2$)	0,694	0,722
sum power band + MSE + DFA ($\alpha_1 + \alpha_2$) **+ LZ**	0,611	0,722
kurtosis + DFA ($\alpha_1 + \alpha_2$)	0,611	0,722
kurtosis + MSE + DFA ($\alpha_1 + \alpha_2$)	0,694	0,778
kurtosis + MSE + DFA ($\alpha_1 + \alpha_2$) **+ LZ**	0,667	0,750
mean + MSE + DFA ($\alpha_1 + \alpha_2$)	0,778	0,722
mean + MSE + DFA ($\alpha_1 + \alpha_2$) **+ LZ**	0,611	0,750
spectral skewness + MSE + DFA ($\alpha_1 + \alpha_2$) **+ LZ**	0,667	0,667
spectral spread + MSE	0,667	0,694
spectral spread + MSE + DFA ($\alpha_1 + \alpha_2$) **+ LZ**	0,639	0,722
Right Forearm		
spectral spread + MSE + DFA ($\alpha_1 + \alpha_2$) **+ LZ**	0,750	0,722
mean + MSE + DFA ($\alpha_1 + \alpha_2$) **+ LZ**	0,778	0,694
spectral kurtosis + MSE + DFA ($\alpha_1 + \alpha_2$)	0,722	0,778
spectral kurtosis + MSE + DFA ($\alpha_1 + \alpha_2$) **+ LZ**	0,750	0,806
spectral spread + MSE + DFA ($\alpha_1 + \alpha_2$)	0,778	0,722
Right Arm		
MSE + coherence	0,778	0,722
MSE + coherence + DFA ($\alpha_1 + \alpha_2$)	0,722	0,778
sum power band + MSE + coherence + DFA ($\alpha_1 + \alpha_2$)	0,639	0,778
sum power band + MSE + coherence + PLF + DFA ($\alpha_1 + \alpha_2$)	0,750	0,806
kurtosis + DFA ($\alpha_1 + \alpha_2$)	0,611	0,694
kurtosis + MSE + DFA ($\alpha_1 + \alpha_2$)	0,750	0,806
kurtosis + MSE + DFA ($\alpha_1 + \alpha_2$) **+ LZ**	0,806	0,778
kurtosis +MSE + coherence + PLF + DFA ($\alpha_1 + \alpha_2$)	0,833	0,694
max frequency + DFA ($\alpha_1 + \alpha_2$)	0,722	0,611
max frequency + MSE + DFA ($\alpha_1 + \alpha_2$)	0,722	0,694
max frequency + MSE + DFA ($\alpha_1 + \alpha_2$) **+ LZ**	0,694	0,694
max frequency + MSE + coherence + DFA ($\alpha_1 + \alpha_2$)	0,611	0,806
mean + MSE + DFA ($\alpha_1 + \alpha_2$)	0,806	0,639
mean + MSE + DFA ($\alpha_1 + \alpha_2$) **+ LZ**	0,722	0,667
mean + MSE + coherence + PLF + DFA ($\alpha_1 + \alpha_2$)	0,778	0,694
spectral kurtosis + DFA ($\alpha 1 + \alpha_2$)	0,722	0,778
spectral kurtosis + MSE + DFA ($\alpha_1 + \alpha_2$) **+ LZ**	0,778	0,750
spectral kurtosis + MSE + coherence + PLF + DFA ($\alpha_1 + \alpha_2$)	0,778	0,694
spectral skewness + MSE	0,639	
spectral skewness + MSE + coherence + DFA ($\alpha_1 + \alpha_2$)	0,861	0,750
spectral spread + coherence	0,667	0,778
spectral spread + MSE + coherence + DFA ($\alpha_1 + \alpha_2$)	0,694	0,778
spectral spread + MSE + coherence + PLF + DFA ($\alpha_1 + \alpha_2$)	0,833	0,694
All features	0,694	0,778

Table B.3: Classification results for the right arm for Naïve Bayes Classifier .

Combinations	**Naïve Bayes**
Right Hand	
LZ	0,639
MSE + FD + LZ + DFA ($\alpha_1 + \alpha_2$)	0,500
sum power band + MSE + DFA ($\alpha_1 + \alpha_2$)	0,278
sum power band + MSE + DFA ($\alpha_1 + \alpha_2$) **+ LZ**	0,278
kurtosis + DFA ($\alpha_1 + \alpha_2$)	0,667
kurtosis + MSE + DFA ($\alpha_1 + \alpha_2$)	0,639
kurtosis + MSE + DFA ($\alpha_1 + \alpha_2$) **+ LZ**	0,667
mean + MSE + DFA ($\alpha_1 + \alpha_2$)	0,611
mean + MSE + DFA ($\alpha_1 + \alpha_2$) **+ LZ**	0,639
spectral skewness + MSE + DFA ($\alpha_1 + \alpha_2$) **+ LZ**	0,556
spectral spread + MSE	0,611
spectral spread + MSE + DFA ($\alpha_1 + \alpha_2$) **+ LZ**	0,639
Right Forearm	
spectral spread + MSE + DFA ($\alpha_1 + \alpha_2$) **+ LZ**	0,639
mean + MSE + DFA ($\alpha_1 + \alpha_2$) **+ LZ**	0,694
spectral kurtosis + MSE + DFA ($\alpha_1 + \alpha_2$)	0,722
spectral kurtosis + MSE + DFA ($\alpha_1 + \alpha_2$) **+ LZ**	0,722
spectral spread + MSE + DFA ($\alpha_1 + \alpha_2$)	0,639
Right Arm	
MSE + coherence	0,694
MSE + coherence + DFA ($\alpha_1 + \alpha_2$)	0,667
sum power band + MSE + coherence + DFA ($\alpha_1 + \alpha_2$)	0,611
sum power band + MSE + coherence + PLF + DFA ($\alpha_1 + \alpha_2$)	0,722
kurtosis + DFA ($\alpha 1 + \alpha_2$)	0,694
kurtosis + MSE + DFA ($\alpha_1 + \alpha_2$)	0,694
kurtosis + MSE + DFA ($\alpha_1 + \alpha_2$) **+ LZ**	0,694
kurtosis +MSE + coherence + PLF + DFA ($\alpha 1 + \alpha 2$)	0,722
max frequency + DFA ($\alpha_1 + \alpha_2$)	0,778
max frequency + MSE + DFA ($\alpha_1 + \alpha_2$)	0,778
max frequency + MSE + DFA ($\alpha_1 + \alpha_2$) **+ LZ**	0,778
max frequency + MSE + coherence + DFA ($\alpha_1 + \alpha_2$)	0,667
mean + MSE + DFA ($\alpha_1 + \alpha_2$)	0,778
mean + MSE + DFA ($\alpha_1 + \alpha_2$) **+ LZ**	0,778
mean + MSE + coherence + PLF + DFA ($\alpha_1 + \alpha_2$)	0,722
spectral kurtosis + DFA ($\alpha_1 + \alpha_2$)	0,639
spectral kurtosis + MSE + DFA ($\alpha_1 + \alpha_2$) **+ LZ**	0,639
spectral kurtosis + MSE + coherence + PLF + DFA ($\alpha_1 + \alpha_2$)	0,667
spectral skewness + MSE	0,639
spectral skewness + MSE + coherence + DFA ($\alpha_1 + \alpha_2$)	0,667
spectral spread + coherence	0,639
spectral spread + MSE + coherence + DFA ($\alpha_1 + \alpha_2$)	0,667
spectral spread + MSE + coherence + PLF + DFA ($\alpha_1 + \alpha_2$)	0,722
All features	0,611

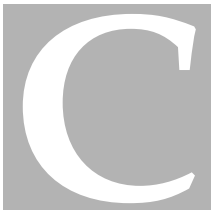

Appendix C

On this appendix is presented an abstract and a poster entitled 'Estudo do comportamento dinâmico do sinal em neuropatias'. They were submitted and accepted in conference FÍSICA 2014 – 19^a Conferência Nacional de Física and represent the work and the results obtained in this thesis. It is also presented the abstract of a paper entitled 'Electromyographic signal dynamic behavior in neuropathies: spectral parameters evaluation and classification'. This paper was submitted to BIOSIGNALS 2015 conference.

ESTUDO DO COMPORTAMENTO DINÂMICO DO SINAL ELETROMIOGRÁFICO EM NEUROPATIAS

Maria Marta Santos[1,2], Ana Luísa Gomes[1, 2], Hugo Gamboa[1,2], Mamede de Carvalho[3], Susana Pinto[3], Carla Quintão[1,4]

[1]Faculdade de Ciências e Tecnologia, Universidade Nova de Lisboa
[2]PLUX - Wireless Biosignals, Lisboa, Portugal
[3]Faculdade de Medicina- Instituto de Medicina Molecular, Universidade de Lisboa
[4]Instituto de Biofísica e Engenharia Biomédica, Faculdade de Ciências, Universidade de Lisboa
mmo.santos@campus.fct.unl.pt

RESUMO

A Esclerose Lateral Amiotrófica é uma doença caracterizada pela degeneração progressiva de neurónios motores, que reduz a força muscular. Neste projeto, recorre-se a técnicas de processamento de sinal em tempo/frequência e a ferramentas que avaliam o comportamento dinâmico do sinal para caracterizar o registo eletromiográfico de superfície destes pacientes e compará-lo com um grupo de controlo. Os registos foram feitos em músculos dos membros superiores e a análise feita para aquisições ipsilaterais. Os resultados preliminares indicam a análise da Coerência e da Multiscale Entropy como os melhores métodos de separação entre populações, verificando-se coerências e entropias mais elevadas para controlos.

ESTUDO DO COMPORTAMENTO DINÂMICO DO SINAL ELETROMIOGRÁFICO EM NEUROPATIAS

Maria Marta Santos[1,2], Ana Luísa Gomes[1, 2], Hugo Gamboa[1,2], Mamede de Carvalho[3], Susana Pinto[3], Carla Quintão[1,4]

[1]Faculdade de Ciências e Tecnologia, Universidade Nova de Lisboa, [2]PLUX - Wireless Biosignals, Lisboa, Portugal, [3]Faculdade de Medicina- Instituto de Medicina Molecular, Universidade de Lisboa, [4]Instituto de Biofísica e Engenharia Biomédica, Faculdade de Ciências, Universidade de Lisboa

Introdução

- A Esclerose Lateral Amiotrófica (ELA) é uma doença caracterizada pela degeneração progressiva de neurónios motores, que reduz a força muscular, sendo muito difícil de ser diagnosticada.
- Neste trabalho são usados métodos matemáticos tais como Coerência, Phase Locking Factor (PLF), Dimensão Fratal (DF) e Comprimento Fratal Máximo, técnicas de Lempel-Ziv (LZ), Detrended Fluctuation Analysis (DFA) e Multiscale Entropy (MSE), de forma a caracterizar o sinal eletromiográfico de superfície (sEMG) de pacientes com ELA, com o objetivo de avaliar a sincronização de diferentes grupos musculares, assim como de analisar o comportamento caótico e a complexidade do sinal.
- Finalmente é aplicado um algoritmo de classificação aos resultados obtidos.
- O objetivo principal será o de distinguir pacientes com ELA de indivíduos saudáveis.

Métodos

Indivíduos

- Foram realizadas simultaneamente aquisições contralaterais e ipsilaterais nas mãos e antebraços.
- O estudo foi realizado com 18 pacientes e 26 indivíduos no grupo de controlo.

Aquisição de sinal

- O sinal sEMG foi adquirido recorrendo a uma unidade *bioPLUXresearch*. A aquisição foi feita para 4 canais a uma frequência de amostragem de 1000 Hz.
- Os elétrodos foram colocados no primeiro interósseo dorsal e no músculo extensor dos dedos para cada lado do corpo.

Protocolo de aquisição

Na **Figura 1** é possível observar a tarefa realizada pelos indivíduos, com 3 s de contração e 3 s de relaxação.

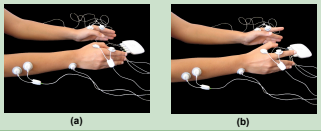

(a) (b)

Figura 1: *Bioplux research device*, posicionamento de quatro elétrodos e do elétrodo de terra. **(a)** Instante de relaxação. **(b)** Instante de contração.

Processamento de sinal

- Os sinais adquiridos foram processados utilizando linguagem *python*.
- Inicialmente foi aplicado um filtro passa banda de 10—500 Hz de terceira ordem.
- Os momentos de contração foram isolados **[1]**.
- Para avaliar a sincronização de diferentes grupos musculares foram calculados a coerência e o PLF entre os diversos registos **[1]**.
- Para analisar o comportamento caótico do sinal determinou-se a DF **[2]** e o Comprimento Fratal Máximo **[3]** e a MSE **[4]**.
- A complexidade do sinal foi avaliada com base na DFA **[2]**, e no algoritmo de LZ **[5]**.
- O algoritmo de classificação foi adaptado de **[6]**.

Resultados

A **Figura 2** apresenta os resultados para a coerência para ambos os membros superiores. Verifica-se uma coerência ligeiramente maior para o grupo de controlo para a banda alfa, embora estatisticamente estas diferenças só sejam significativas com um baixo grau de confiança.

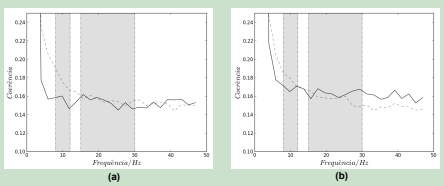

(a) (b)

Figura 2: Média da coerência em função da frequência para o grupo de pacientes (linha contínua) e para o grupo de controlo (linha a tracejado). A cinzento encontram-se representadas as frequências correspondentes à banda alfa (8—12 Hz) e à banda beta (15—30 Hz) **(a)** Resultados para o membro superior esquerdo. **(b)** Resultados para o membro superior direito.

A **Figura 3** apresenta os resultados para o PLF para ambos os membros superiores. Verifica-se um PLF ligeiramente mais elevado para o grupo de controlo para a banda alfa, embora estatisticamente estas diferenças só sejam significativas com um baixo grau de confiança.

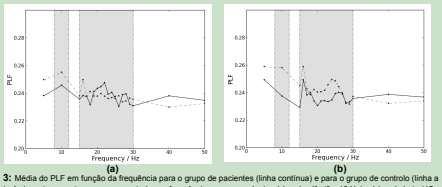

(a) (b)

Figura 3: Média do PLF em função da frequência para o grupo de pacientes (linha contínua) e para o grupo de controlo (linha a tracejado). A cinzento encontram-se representadas as frequências correspondentes à banda alfa (8—12 Hz) e à banda beta (15—30 Hz). **(a)** Resultados para o membro superior esquerdo. **(b)** Resultados para o membro superior direito.

A **Tabela 1** apresenta os resultados para o algoritmo de DF para os membros superiores para ambos os grupos. A **Tabela 2** apresenta o Comprimento Fratal Máximo para os membros superiores para ambos os grupos.

Tabela 1: Valores médios e de desvio padrão de DF para o grupo de pacientes e para o grupo de controlo.

	Grupo de pacientes	Grupo de controlo
Mão esq.	-1.984 ± 0.011	-1.983 ± 0.007
Antebraço esq.	-1.982 ± 0.008	-1.983 ± 0.006
Mão dir.	-1.985± 0.008	-1.983 ± 0.008
Braço dir.	-1.983 ± 0.013	-1.984 ± 0.006

Tabela 2: Valores médios e de desvio padrão do Comprimento Fratal Máximo para o grupo de pacientes e para o grupo de controlo.

	Grupo de pacientes	Grupo de controlo
Mão esq.	3.80± 0.29	3.98 ± 0.20
Antebraço esq.	3.70 ± 0.42	3.74 ± 0.27
Mão dir.	3.72 ± 0.39	3.99 ± 0.20
Antebraço dir.	3.72 ± 0.47	3.80 ± 0.22

A **Tabela 3** apresenta os resultados para o algoritmo de LZ para ambos os membros superiores. A sequência binária usada no algoritmo de LZ foi obtida a partir da retificação de onda completa do sinal filtrado com limiar 0.4.

Tabela 3: Valores médios e de desvio padrão para o coeficiente de LZ para o grupo de pacientes e para o grupo de controlo.

	Grupo de pacientes	Grupo de controlo
Mão esq.	0.22 ± 0.17	0.28 ± 0.19
Antebraço esq.	0.24 ± 0.20	0.16 ± 0.12
Mão dir.	0.17 ± 0.13	0.27± 0.16
Antebraço dir.	0.27 ± 0.29	0.16 ± 0.13

As **Tabelas 4 e 5** apresentam os resultados para o algoritmo de DFA para ambos os membros superiores para o grupo de pacientes e o grupo de controlos.

Tabela 4: Valores médios e de desvio padrão para o coeficiente α_1 de DFA para ambos os grupos.

	Grupo de pacientes	Grupo de controlo
Mão esq.	1.24 ± 0.20	1.38 ± 0.16
Anteraço esq.	1.36 ± 0.28	1.43 ± 0.15
Mão dir.	1.23 ± 0.17	1.35 ± 0.14
Antebraço dir.	1.39 ± 0.09	1.44 ± 0.11

Tabela 5: Valores médios e de desvio padrão para o coeficiente α_2 de DFA para ambos os grupos.

	Grupo de pacientes	Grupo de controlo
Mão esq.	0.48 ± 0.11	0.52 ± 0.10
Antebraço esq.	0.60 ± 0.14	0.67 ± 0.13
Mão dir.	0.50 ± 0.12	0.52 ± 0.09
Antebraço dir.	0.62 ± 0.16	0.59 ± 0.10

A **Figura 4** apresenta os resultados para o algoritmo de MSE para o membro superior direito. Os resultados para o membro superior esquerdo são semelhantes. Foram utilizadas 20 escalas, sendo a tolerância utilizada $r=0.15\sigma$.

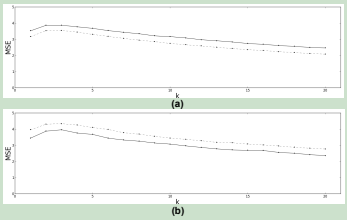

(a) (b)

Figura 4: Média da MSE para cada escala para o grupo de pacientes (linha contínua) e para o grupo de controlo (linha a tracejado). **(a)** Resultados para a mão direita. **(b)** Resultados para o antebraço direito.

Verificam-se entropias mais elevadas para os pacientes para as mãos e mais elevadas para os controlos para os antebraços, embora estatisticamente estas diferenças só sejam significativas com um baixo grau de confiança.

O algoritmo de classificação apresenta uma boa capacidade de distinção entre ambos os grupos, e de 201 combinações feitas, em 118 combinações o algoritmo acertou em mais de 70% dos casos.

Conclusão

- Os algoritmos de LZ, DFA e MSE apresentam uma boa capacidade de distinção entre o grupo de controlo e o grupo de pacientes. Os resultados da classificação demonstram capacidade de distinção entre ambos os grupos. Estes resultados podem demonstrar-se importantes no diagnóstico da doença, sendo que a utilização de sEMG aparenta ser um método promissor como auxiliar de diagnóstico.

Referências

[1] Mahdeia Camara. Coherence and phase locking disruption in electromyograms of patients with amyotrophic lateral sclerosis. Master's thesis, Faculdade de Ciências e Tecnologia da Universidade Nova de Lisboa, 2013.
[2] Angkoon Phinyomark, Pornchai Phukpattaranont, Chusak Limsakul, and Montri Phothisonothai. Electromyography (emg) signal classification based on detrended fluctuation analysis. *Fluctuation and Noise Letters*, 10(03):281–301, 2011.
[3] Sridhar Poosapadi Arjunan and Dinesh Kant Kumar. Computation of fractal features based on the fractal analysis of surface electromyogram to estimate force of contraction of different muscles. *Computer Methods in Biomechanics and BiomedicalEngineering*, 17(3):210–216, 2014.
[4] Yu-Hsiang Pan, Wei-Yen Lin, Yung-Hung Wang, and Kuo-Tien Lee. Computing multiscale entropy with orthogonal range search. *Journal of Marine Science and Technology*, 19(1):1.7-113, 2011.
[5] Leonardo Serlavóus, Abel Torres, José A. Fo, Josep Rivera, and Raimon Jané. Index for estimation of muscle force from mechanomyography based on lempel-ziv algorithm. *Journal of Electromyography and Kinesiology*, 2013.
[6] Ana Luísa Gomes. Advanced Accelerometry Signal Processing for Human Activity Recognition. Master's thesis, Faculdade de Ciências e Tecnologia da Universidade Nova de Lisboa, 2014 (in press).

Agradecimentos

Este trabalho teve suporte financeiro da Fundação para a Ciência e a Tecnologia através do projeto estratégico com referência: PEst-OE/SAU/UI0645/2014.

Electromyographic signal dynamic behavior in neuropathies: spectral parameters evaluation and classification

Maria Marta Santos[1,2], Ana Luísa Gomes[1,2], Hugo Gamboa[1,2], Mamede de Carvalho[3], Susana Pinto[3], Carla Quintão[1,4]

[1]*Faculdade de Ciências e Tecnologia, Universidade Nova de Lisboa*

[2]*PLUX - Wireless Biosignals, Lisboa, Portugal*

[3]*Faculdade de Medicina- Instituto de Medicina Molecular, Universidade de Lisboa*

mmo.santos@campus.fct.unl.pt, alg.gomes@campus.fct.unl.pt, hgamboa@plux.info, mamedemg@netcabo.pt, susana.c.pinto@sapo.pt, cmquintao@fct.unl.pt

Keywords: Amyotrophic Lateral Sclerosis (ALS), Coherence, Phase Locking Factor (PLF), Fractal Dimension (FD), Lempel-Ziv (LZ), Detrended Fluctuation Analysis (DFA), Multiscale Entropy (MSE) , Surface Electromyography (sEMG), Ipsilateral, Classification.

Abstract: Amyotrophic Lateral Sclerosis (ALS) is a neurodegenerative disease characterized by motor neurons degeneration, which reduces muscular force, being very difficult to diagnose. Mathematical methods, such as Coherence, Phase Locking Factor (PLF), Fractal Dimension (FD), Lempel-Ziv (LZ) techniques, Detrended Fluctuation Analysis (DFA) and Multiscale Entropy (MSE) are used to analyze the surface electromiographic signal's chaotic behavior and evaluate different muscle groups' synchronization. Surface electromiographic signal acquisitions were performed in upper limb muscles, being the analysis executed for instants of contraction for ipsilateral acquisitions for patients and control groups. Results from LZ, DFA and MSE analysis present capability to distinguish between the patient and the control groups, whereas coherence, PLF and FD algorithms present results very similar for both groups. LZ, DFA and MSE algorithms appear then to be a good measure of corticospinal pathways integrity. A classification algorithm was applied to the results in combination with extracted features from the surface electromiographic signal, with an accuracy percentage higher than 70% for 118 combinations for at least one classifier. The classification results demonstrate capability to distinguish both groups. These results can demonstrate a major importance in the disease diagnose, once surface electromyography (sEMG) may be used as an auxiliary diagnose method.